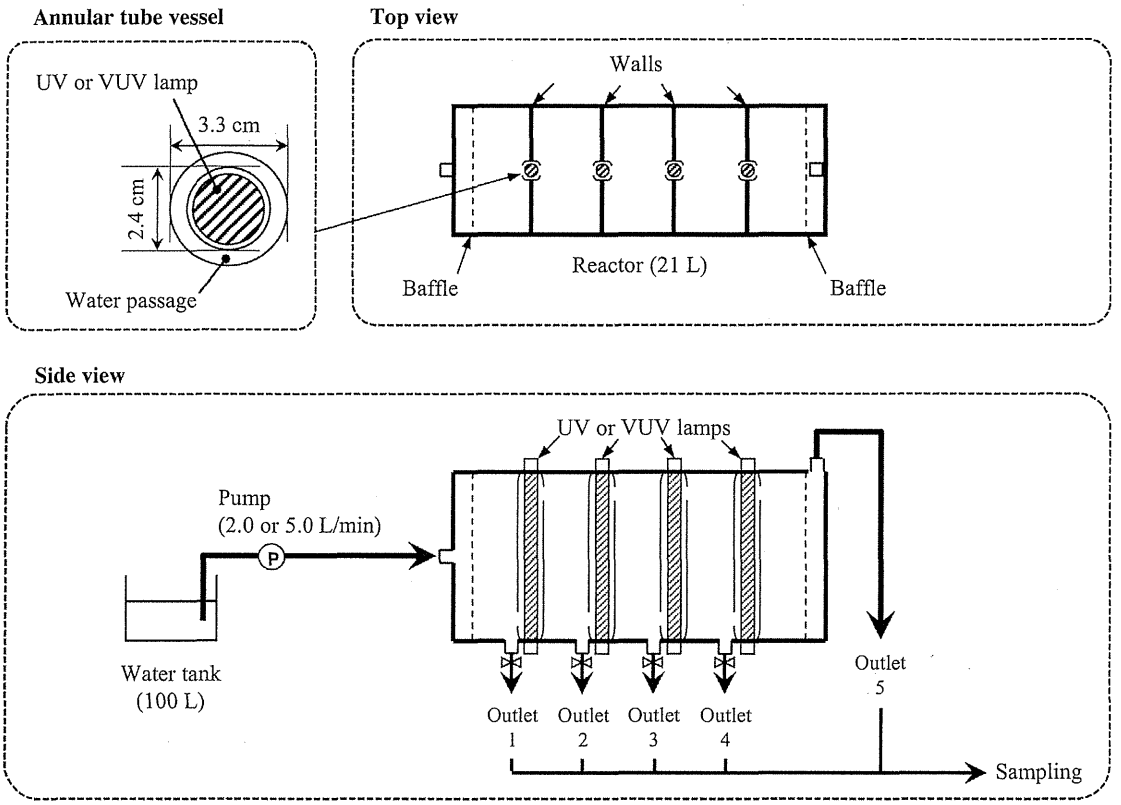

Fig. 2 – Experimental setup 2, photolysis reactor operated in one-pass mode.

groundwater was used mainly for feasibility studies: specifically, the decomposition of 1,4-dioxane, the effect of added H_2O_2, and by-product formation from NOM and nitrate were investigated with the groundwater.

The lake water was collected from Lake Hakucho (Tomakomai, Japan) on November 20, 2012, and was stored at 4 °C until use. The area upstream of the lake is covered with broad-leaved forest and swamp grassland, and therefore the lake water has a high proportion of NOM relative to anthropogenic organic matter. The lake water was filtered with a glass fiber filter ($\phi = 0.5\,\mu m$, GB-140, Toyo Roshi Kaisha, Tokyo, Japan) to remove suspended solids prior to use in the experiments. The lake water was used to investigate by-product formation from NOM and nitrate.

Chemicals added to the water samples were purchased from Wako Pure Chemical Industries (Osaka, Japan) and used as supplied without further purification.

2.4. *Experimental setup 1*

Decomposition of 1,4-dioxane, the effects of the TiO_2 photocatalyst and pH, and bromate formation from bromide were investigated with ES1 (Fig. 1). ES1 consisted of a water tank, a pump, and a photocatalysis reactor (Aquasolution, Ube Industries, Tokyo, Japan) and was operated in circulation mode. The volume of the reactor was 7.5 L. Four evenly spaced lamp inserts were located along the center line of the reactor, and either VUV lamp 1 or UV lamp 1, which had been turned on and allowed to warm up prior to the experiment, was installed in each insert. The reactor was equipped with five evenly spaced slots into which the fabric photocatalyst sheets were installed.

The water tank was charged with 10 L of buffered DTW, which was then pumped into the reactor at a constant flow rate of 5.0 L/min. The water passed through the photocatalyst sheets in the flow direction when the sheets were installed. The irradiated water then returned to the water tank, where it was completely mixed with a mechanical stirrer. Samples were periodically withdrawn from a three-way stopcock, and the concentrations of 1,4-dioxane, 2-MIB, and geosmin in the samples were measured.

Overall irradiation time (T, min) in the continuous decomposition experiments conducted in circulation mode was calculated as follows:

$$T = \frac{V_t}{V} \cdot t \tag{1}$$

where t is the sampling time (min), V_t is the volume of the water at sampling time t (L), and V is the volume of the reactor (L).

Table 2 – Water samples used.

	DOC mg/L	OD260 cm^{-1}	Turbidity NTU	pH
Buffered dechlorinated tap water	0.7	0.003	0	5.5–8.0
Groundwater	0.2	0.001	0	7.8
Lake water	2.6	0.098	8.1	7.6

For comparison of the results obtained with the two different ESs, the apparent decomposition rate constants (k) were standardized by the electric power consumption of the VUV or UV lamps: k values were determined from the slopes of plots of $\ln(C_T/C_0)$ versus the electric power consumption of the system per unit volume of water (E, J/L) (Eq. (2)):

$$\ln \frac{C_T}{C_0} = -kE \tag{2}$$

where C_T is the concentration of the target compound at overall irradiation time T and C_0 is the initial concentration of the target compound. E was calculated as follows:

$$E = \frac{nP}{V} \cdot 60T \tag{3}$$

where n is the number of lamps (dimensionless), and P is the electric power per lamp (W).

2.5. Experimental setup 2

The effect of H_2O_2 on 1,4-dioxane removal, aldehyde formation from NOM, and nitrite formation from nitrate were investigated with ES2 (Fig. 2). ES2 consisted of a water tank, a pump, and a photolysis reactor (Aquasolution, Ube Industries) and was operated in one-pass mode. The water tank was charged with groundwater (100 L), which was then pumped into the reactor at a constant flow rate of 5.0 L/min. To enhance the efficiency of VUV irradiation, we used a reactor that differed from that used for ES1 as follows. The reactor (volume, 21 L) was vertically divided into five equal-volume chambers by walls equipped with annular tube vessels through which the water had to pass to flow to the next chamber. The vessels were made of quartz silica that transmitted both UV and VUV light. The internal and external diameters of the vessels were 2.4 and 3.3 cm, respectively. Lamps, either VUV lamp 2 or UV lamp 2, that had been turned on and allowed to warm up prior to the experiment were inserted in the internal wall of the vessels. The water passed between the internal and external walls from the bottom to the top, and then to the next chamber: thus, the water was forced to flow in close proximity to the lamps. Because water molecules readily absorb VUV light, hydroxyl radicals are generated only in a very thin water layer close to the lamp surface (i.e., just outside the lamp sleeve). Moreover, because the diffusion coefficient of hydroxyl radicals is 2.3×10^{-5} cm^2/s (LaVerne, 1989) and its lifetime in water is short (10^{-9}–10^{-6} s (LaVerne, 1989)), the hydroxyl radicals were expected to be involved in reactions only in the immediate vicinity of where they were generated (i.e., only around the lamp sleeve). Finally, the treated water was discharged from outlet 5. Samples were withdrawn from outlets 1–5, and the concentrations of 1,4-dioxane in the samples were measured. Dividing the concentrations of 1,4-dioxane in the samples from outlets 1–5 by the concentration in the samples from outlet 1 gave the residual ratios.

Decomposition rate constants were determined as described in Section 2.4: that is, k values were determined from the slopes of plots of $\ln(C_T/C_0)$ versus E (Eq. (2)). E (J/L) was calculated as follows:

$$E = 60 \cdot \frac{nP}{v} \tag{4}$$

where n is the number of lamps by which the raw water had been irradiated (n = 1, 2, 3, and 4 for outlets 2, 3, 4, and 5, respectively), and v is the flow rate of the raw water (L/min).

2.6. By-product formation and its control by GAC treatment

VUVBPs and CDBPFP were investigated with ES2. The water tank was charged with either lake water or groundwater (100 L), which was then pumped into the reactor at a constant flow rate of 2.0 L/min in one-pass mode. The VUV-treated water was collected from outlet 5. In a preliminary experiment, we confirmed that the experimental conditions, including the VUV dose, were sufficient to remove 1,4-dioxane: specifically, the 1,4-dioxane concentration in the groundwater dropped from approximately 100 μg/L to less than 10 μg/L, which is lower than the WHO drinking water guideline (50 μg/L) and the Japan regulation value (50 μg/L). Under these conditions, the electric power consumption rate was calculated to be 7.8 kJ/L, which was much lower than the rates reported by Buchanan et al. (2006) (3.2×10^2–3.7×10^3 kJ/L) whose main target was high concentration of NOM.

To investigate GAC adsorption of the VUVBPs, we used two types of GAC: a virgin GAC and a used GAC. The virgin GAC (coal-based GAC, LG-20S, Swing Corp., Tokyo, Japan) was washed thoroughly with Milli-Q water to remove impurities and then dried in an oven at 103 °C overnight, cooled to room temperature, and stored in a desiccator until use. The used GAC was a coal-based GAC (Shanxi Xinhua Protective Equipment, Taiyuan, China) that had been in service for 6 years in a full-scale drinking water treatment plant in Tokyo and had been collected when the GAC bed was replaced. This spent adsorbent, which might possess biological activity, was expected to act as BAC (hereafter, BAC). The BAC was washed thoroughly with Milli-Q water to remove impurities. Either BAC or virgin GAC was packed to a bed depth of 100 cm in an acrylic column with an internal diameter of 1.5 cm. The VUV-treated water was fed into BAC and GAC columns at a constant flow rate of 16 mL/min (10 min of contact time) by peristaltic pumps. The column effluent was collected on days 11 and 12 of operation. VUVBPs and the CDBPFP were almost the same in the samples withdrawn on two days. 1,4-Dioxane remaining in the VUV-treated water completely broke through the virgin GAC bed by day 11 of operation. Therefore, samples were collected after the GAC bed was pseudo-stabilized. On the other hand, the BAC column had been already broken through in terms of 1,4-dioxane at the beginning of the filtration. The data provided in Section 3 are averages of the concentrations in the samples collected on days 11 and 12.

To determine CDBPFP, we supplemented aliquots of raw water, VUV-treated water, and VUV/GAC-treated water with sodium hypochlorite (Asahi Glass Co., Tokyo, Japan) in an amount sufficient to result in a residual free chlorine concentration of 1–2 mg-Cl_2/L after 24 h. The vessels containing the chlorinating water samples were tightly sealed to prevent vaporization of chlorine and the by-products and were incubated in the dark at 20 °C for 24 h.

2.7. Quantification methods

Concentrations of 1,4-dioxane, 2-MIB, and geosmin were measured by gas chromatography/mass spectrometry (GC/MS) on a QP2010 Plus instrument (Shimadzu Co., Kyoto, Japan) coupled to a purge-and-trap pretreatment system (Aqua PT 5000J

Plus, AQUAauto 70, GL Science Inc., Tokyo, Japan) and a capillary column (length, 30 m; i.d., 250 μm; thickness, 0.25 μm; HP-5 ms, Agilent Technologies, Palo Alto, CA, USA). GC/MS was performed in selected ion monitoring (SIM) mode with geosmin-d_3 and 1,4-dioxane-d_8 as internal standards. The detected fragment ions (*m/z*) of the compounds were as follows: 1,4-dioxane, 88; 2-MIB, 95; geosmin, 112; 1,4-dioxane-d_8, 96; geosmin-d_3, 115.

Bromoform, dibromochloromethane (DBCM), bromodichloromethane (BDCM), and chloroform in the chlorinated waters were quantified by GC/MS (QP2010 Plus) with a purge-and-trap sample concentrator (AQUA PT 5000J Plus). A capillary column (length, 60 m; i.d., 250 μm; thickness, 0.25 μm; InertCap AQUATIC, GL Sciences) was used for sample separation. GC/MS was performed in SIM mode.

Nine HAAs (bromoacetic acid (BAA), chloroacetic acid (CAA), dibromoacetic acid (DBAA), bromochloroacetic acid (BCAA), dichloroacetic acid (DCAA), tribromoacetic acid (TBAA), dibromochloroacetic acid (DBCAA), bromodichloroacetic acid (BDCAA), and trichloroacetic acid (TCAA)) were extracted from the chlorinated waters by a liquid–liquid extraction method with methyl *tert*-butyl ether, derivatized with *N*-methyl-*N*′-nitro-*N*-nitrosoguanidine according to Standard Methods for the Examination of Water (JWWA, 2011), and quantified by GC/MS (7890A GC/5975C MS, Agilent Technologies). A capillary column (length, 30 m; i.d., 250 μm; thickness, 1.0 μm; DB-5MS, Agilent Technologies) was used for sample separation. GC/MS was performed in SIM mode.

Ten aldehydes (formaldehyde, propanal, butanal, pentanal, hexanal, heptanal, octanal, nonanal, benzaldehyde, and glyoxal) and 1,4-dioxane were quantified by GC/MS (QP2010 Plus) with a purge-and-trap sample concentrator (AQUA PT 5000J Plus). A capillary column (InertCap AQUATIC) was used for sample separation. GC/MS was performed in SIM mode. Because acetaldehyde could not be quantified reproducibly, it was not considered in the present study; it was detected in some samples, possibly as a result of contamination from the acrylic column used or from the atmosphere.

Bromate concentration was measured with a high-performance liquid chromatograph combined with an electrospray ionization tandem mass spectrometer (API3000, AB Sciex Instruments, Foster City, CA, USA) or a hybrid quadrupole-orbitrap mass spectrometer (Q Exactive, Thermo Fisher Scientific Inc., Waltham, MA, USA). Bromide, nitrate, and nitrite concentrations were measured with an ion chromatograph (DX-120, Dionex, Sunnyvale, CA, USA) equipped with a separation column (IonPac AS14, Dionex).

3. Results and discussion

3.1. *Decomposition of 1,4-dioxane by VUV treatment and effect of TiO_2 on the decomposition*

We evaluated the changes in the residual ratios of 1,4-dioxane, 2-MIB, and geosmin at pH 7.0 with ES1 (Fig. 3). No decrease in the residual ratios was observed in the control experiments (no photocatalyst in the dark, gray diamonds), which implies that adsorption on the apparatus and evaporation were negligibly small. Under UV irradiation (gray triangles), the residual ratios for all the target compounds decreased, but only slightly, indicating that the extent of direct UV photolysis was limited. Slight reductions in the amounts of 2-MIB and geosmin under UV irradiation have been reported previously (Kutschera et al., 2009; Rosenfeldt et al., 2005), in agreement with our observations.

UV irradiation with the photocatalyst (white triangles) increased the decomposition of the target compounds relative to that in the absence of the photocatalyst. Decomposition of 1,4-dioxane by irradiation with xenon lamps (Maurino et al., 1997) and low-pressure mercury vapor fluorescent lamps (Mehrvar et al., 2002) has been reported to be improved by the addition of TiO_2, which agrees with our results. Rapid degradation of 2-MIB and geosmin by UV/TiO_2 treatment has also been reported (Lawton et al., 2003), which also agrees with our results.

UV irradiation of water in the presence of a TiO_2 photocatalyst generates positive holes (h^+) and hydroxyl radicals (•OH) (Gaya and Abdullah, 2008),

$$TiO_2 + h\nu_{UV} \rightarrow e^- + h^+ \quad (5)$$

$$H_2O + h^+ \rightarrow {}^\bullet OH + H^+ \quad (6)$$

which are expected to play important roles in the decomposition of organic compounds. Additionally, direct photolysis at 254 nm is also expected to contribute to their decomposition. Klečka and Gonsior (1986) reported that 1,4-dioxane is decomposed by Fenton's reaction, during which hydroxyl radicals play a key role. In our system, 1,4-dioxane may have been decomposed mainly by the hydroxyl radicals generated by UV irradiation of the photocatalyst.

All three compounds were effectively decomposed by VUV irradiation (gray circles). To our knowledge, this is the first report of the use of VUV irradiation of water to remove 1,4-dioxane, which is one of the most persistent organic compounds (Zenker et al., 2003). Even though the electric power of the VUV lamps was the same as that of the UV lamps, the target compounds were decomposed to a greater extent with the former than with the latter. Moreover, the extent of decomposition with the VUV lamps in the absence of the photocatalyst was greater than that with the UV lamps in the presence of the photocatalyst. When water is irradiated with the VUV lamps, direct photolysis at 254 nm is expected to be accompanied by water homolysis: irradiation at 185 nm on water has been reported to result in homolysis and hydroxyl radical production (Oppenländer, 2007):

$$H_2O + h\nu_{VUV} \rightarrow {}^\bullet H + {}^\bullet OH \quad (7)$$

Zoschke et al. (2014) reported that these two mechanisms, direct photolysis and decomposition by hydroxyl radicals, are the main contributors to the decomposition of contaminants in water upon VUV irradiation. However, in the present study, the fact that the extent of direct UV photolysis was limited and that decomposition of the target compounds was greatly improved by VUV irradiation indicates that hydroxyl radicals generated by water homolysis effectively decomposed the target compounds. Kutschera et al. (2009) have reported that decomposition of 2-MIB and geosmin during VUV irradiation is dominated by the radical reaction.

VUV irradiation in the presence of the photocatalyst (white circles) greatly enhanced the decomposition of the target compounds. The enhancement was most likely not due to a photocatalytic reaction caused by VUV light. Water molecules readily absorb VUV light; the absorption coefficient of water for VUV light (λ = 184.9 nm) is reported to be $1.80 \pm 0.01\ cm^{-1}$ at

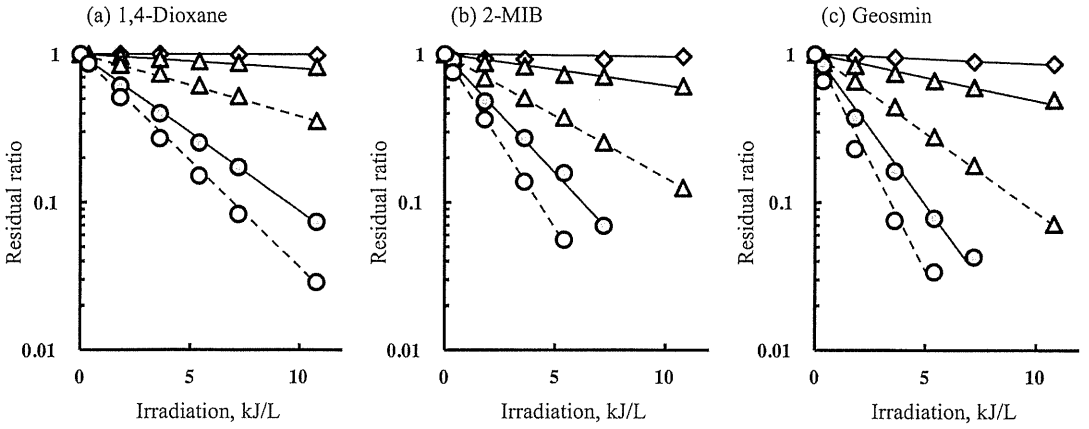

Fig. 3 – Changes in residual ratios of (a) 1,4-dioxane, (b) 2-methylisoborneol (2-MIB), and (c) geosmin during VUV (circles) and UV (triangles) irradiation at pH 7.0 (experimental setup 1, 40 W, circulation mode) in the absence (gray) or presence (white) of photocatalyst. The gray diamonds indicate data for control experiments without photocatalyst in the dark.

20 °C (Weeks and Gordon, 1963). Because the distance between the VUV lamp and the photocatalyst sheet was 3.5 cm in our experimental configuration, the irradiation intensity at the surface of the photocatalyst sheet was quite small, calculated to be at most <0.2% of the irradiation intensity at the surface of the lamp slot. In contrast, the UV absorption coefficient of the raw water used in the present study was measured to be 0.001 cm^{-1} at 254 nm, indicating that unlike VUV light, UV light was not absorbed by the water molecules and thus the photocatalyst received UV light and was excited. Therefore, the decomposition enhancement was most likely due to a UV photocatalytic reaction. The extent of enhancement due to the photocatalyst sheets was smaller for VUV treatment than for UV treatment because the amount of hydroxyl radicals generated by water homolysis upon VUV irradiation was most likely very large compared to the amount generated by photocatalysis.

To compare the efficiencies of the AOPs for 1,4-dioxane decomposition, we calculated EE/O values, that is, the amount of electric energy required to reduce the concentration of a target compound in 1 m^3 of contaminated water by one order of magnitude (Bolton James et al., 2001). EE/O has been used to directly compare treatment AOP-based technologies (Zoschke et al., 2012). EE/O values were calculated as follows (batch operation) (Bolton James et al., 2001):

$$EE/O = \frac{P \cdot t}{V \cdot \log(c_0/c)} \quad (8)$$

where P is electric power (kW), t is time (h), V is reactor volume (m^3), c is 1,4-dioxane concentration at time t, and c_0 is initial 1,4-dioxane concentration. The EE/O values decreased in the order UV > UV/TiO_2 > VUV > VUV/TiO_2 (Table 3). Systems are considered to be economically feasible when the EE/O value is less than 10 (Andrews et al., 1995). On the basis of this criterion, VUV, VUV/TiO_2, and UV/TiO_2 treatments are economically feasible for 1,4-dioxane decomposition, whereas UV treatment is not. However, because the cost of the photocatalyst sheets was not taken into account in the EE/O calculations, the actual EE/O values for VUV/TiO_2 and UV/TiO_2 treatments would be larger than the values shown in Table 3.

Table 3 – Decomposition rate constants (*k*) and EE/O values for 90% decomposition of 1,4-dioxane in buffered dechlorinated tap water.

	k, L/kJ	EE/O, kWh/(m^3 order)
UV	0.057	11
UV/TiO2	0.29	2.2
VUV	0.77	0.83
VUV/TiO2	1.1	0.58

In the present study, 2-MIB decomposed to a lesser extent than geosmin during VUV and UV irradiation both in the presence and absence of the photocatalyst. The same tendency has previously been reported for VUV irradiation (Kutschera et al., 2009; Zoschke et al., 2012). The lower decomposition rates of 2-MIB during VUV, VUV/TiO_2, and UV/TiO_2 treatment were most likely due to the fact that the rate constant for decomposition of 2-MIB by hydroxyl radicals is smaller than that for decomposition of geosmin (Glaze et al., 1990). 1,4-Dioxane decomposed to a lesser extent than did 2-MIB and geosmin in all of the treatments tested in the present study.

3.2. *Effect of pH on decomposition of 1,4-dioxane*

We also investigated the effect of pH on the decomposition rate constants of the target compounds (Fig. 4). The rate constants for the UV/TiO_2 process did not change substantially with pH (white triangles), whereas the rate constants for the VUV (gray circles) and VUV/TiO_2 (white circles) processes showed a relatively large dependence on pH. For all three compounds, the decomposition rate constants were largest at pH 5.5–6.0 and clearly decreased with increasing pH. The decomposition rate constants at pH 5.5–6.0 were roughly twice those at pH 7.5–8.0, indicating that maintaining a pH in the weakly acidic range would facilitate decomposition of these compounds.

VUV irradiation of water results in homolysis and production of hydroxyl radicals (Eq. (7)), which recombine to form H_2O_2 (Oppenländer, 2007):

$$^{\bullet}OH + {}^{\bullet}OH \rightarrow H_2O_2 \quad (9)$$

When H_2O_2 absorbs UV light, hydroxyl radicals are generated by photolysis of the peroxidic bond (Lopez et al., 2003):

$$H_2O_2 + h\upsilon_{UV} \rightarrow {}^{\bullet}OH + {}^{\bullet}OH \quad (10)$$

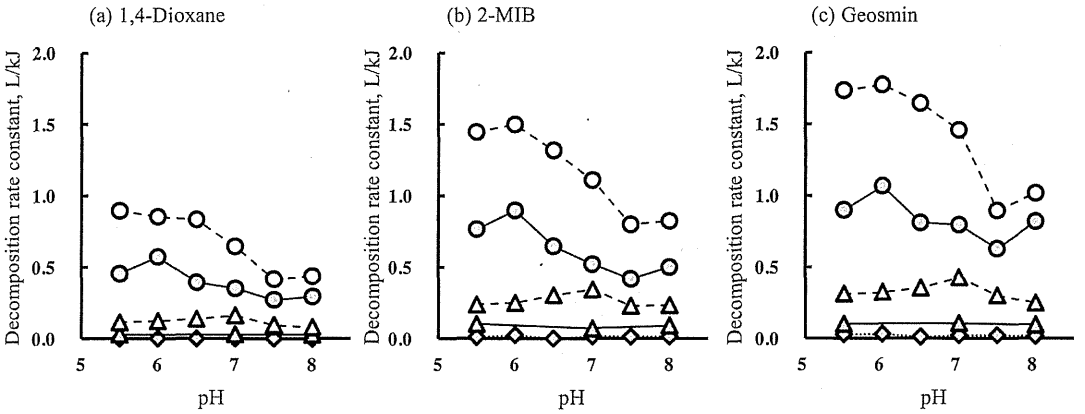

Fig. 4 – Effect of pH on rate constants for decomposition of (a) 1,4-dioxane, (b) 2-methylisoborneol (2-MIB), and (c) geosmin during VUV (circles) and UV (triangles) irradiation (experimental setup 1, 40 W, circulation mode) in the absence (gray) and presence (white) of the photocatalyst. The gray diamonds indicate data for control experiments without photocatalyst in the dark.

Accordingly, under UV light irradiation, hydroxyl radicals and H_2O_2 are in equilibrium:

$$^{\bullet}OH + {}^{\bullet}OH \overset{h\nu_{UV}}{\leftarrow} H_2O_2 \quad (11)$$

H_2O_2 is also in equilibrium with protons and HO_2^- anions (Joyner, 1912):

$$H_2O_2 \leftrightarrow H^+ + HO_2^- \quad (12)$$

High H^+ concentrations (low pH) drive the equilibrium toward the formation of H_2O_2, and its concentration increases accordingly. In turn, increases in the H_2O_2 concentration drive the reaction shown in Eq. (11) toward the formation of hydroxyl radicals. These equilibrium considerations may explain why the decomposition rate constants were higher in the acidic pH range than in the basic pH range.

Alternatively, equilibrium of carbonate may have an influence on the pH-dependence of the decompositions. Carbonate acid, bicarbonate ion and carbonate ion dominate in the equilibrium roughly at low pH (pH < 6), neutral to weak basic pH (6 < pH < 10) and basic pH (pH > 10), respectively. These carbonate species have reportedly scavenging ability of hydroxyl radicals that play a key role during the VUV irradiation, but the extents of the scavenging ability are different and in the order of carbonate acid ≪ bicarbonate ion < carbonate ion (Liao and Gurol, 1995). Accordingly, the equilibrium of carbonate may explain why the decomposition rate constants were higher in the acidic pH range than in the basic pH range.

3.3. *Effect of added H_2O_2 on decomposition of 1,4-dioxane*

Before investigating the effect of added H_2O_2, we evaluated the effect of system configuration by comparing the efficiencies of 1,4-dioxane decomposition using ES1 and ES2 with the same raw water (DTW that was withdrawn on the same day and then spiked with 1,4-dioxane) in the same operation mode (the one-pass mode) at the same flow rate (5.0 L/min). The rate constants for 1,4-dioxane decomposition were calculated to be 0.45 and 2.1 L/kJ for ES1 and ES2 (EE/O = 1.4 and 0.31 kWh/(m^3 order)), respectively; that is, the rate constant for ES2 was approximately 4.5 times that of ES1. Forcing the water to flow in the vicinity of the VUV lamps greatly enhanced the decomposition rate of 1,4-dioxane, indicating that the system configuration is quite important for the design of VUV irradiation setups.

VUV treatment of groundwater in the absence of H_2O_2 (Fig. 5, gray diamonds) decomposed the 1,4-dioxane in the water, and the apparent decomposition rate constant was calculated to be 0.75 L/kJ. This value was much smaller than that in DTW (2.1 L/kJ). Coexisting inorganic and organic materials have been reported to separately affect the decomposition rates of organic pollutants during VUV irradiation; for instance, carbonate and bicarbonate ions reportedly reduce decomposition rates (Imoberdorf and Mohseni, 2012; Kutschera et al., 2009). In our system, the bicarbonate concentration in the groundwater (13.3 mg/L) was much higher than that in the DTW (4.1 mg/L), which likely contributed to suppression of the decomposition rate in the groundwater relative to that in the DTW. Other coexisting materials may have influenced the 1,4-dioxane decomposition in the groundwater; further study of this issue is needed.

Addition of a 1 mg/L dose of H_2O_2 to the VUV system enhanced the decomposition of 1,4-dioxane (Fig. 5, gray triangles): the decomposition rate constant increased by

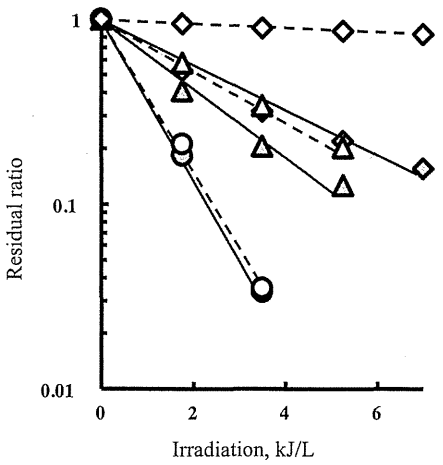

Fig. 5 – Effect of H_2O_2 concentration on 1,4-dioxane decomposition during VUV (circles) and UV (triangles) irradiation (experimental setup 2, 240 W). Diamonds, triangles, and circles indicate data for H2O2 concentrations of 0, 1, and 5 mg/L, respectively.

Table 4 – Decomposition rate constants (k) and EE/O for 90% decomposition of 1,4-dioxane in groundwater.

	k, L/kJ	EE/O, kWh/(m³ order)
VUV	0.75	0.85
VUV + 1 mg/L H2O2	1.1	0.58
VUV + 5 mg/L H2O2	2.7	0.29
UV + 1 mg/L H2O2	0.85	0.76
UV + 5 mg/L H2O2	2.7	0.29

approximately 50%. When the dose of H_2O_2 was increased to 5 mg/L (gray circles), 1,4-dioxane decomposition was accelerated even further: the decomposition rate constant increased to 3.6 times that in the absence of H_2O_2. As mentioned previously, H_2O_2 absorbs VUV and UV light to produce hydroxyl radicals (Eq. (10)), which likely brought about the enhancement in the 1,4-dioxane decomposition.

Although the extent of decomposition of 1,4-dioxane by the UV treatment was quite limited in the absence of H_2O_2 (white diamonds), adding a 1 mg/L dose of H_2O_2 increased the extent of decomposition (white triangles). The decomposition rate constant for UV irradiation with a 1 mg/L dose of H_2O_2 was smaller than that for VUV irradiation with the same H_2O_2 dose but slightly larger than that for VUV treatment alone. When the H_2O_2 dose was increased to 5 mg/L, the UV system effectively decomposed 1,4-dioxane (white circles): the decomposition rate constant was almost the same as that for VUV irradiation with a 5 mg/L dose of H_2O_2. At the lower H_2O_2 dose, VUV/H_2O_2 treatment was more effective than UV/H_2O_2 treatment. However, as the H_2O_2 dose was increased, the difference between the two treatments became negligibly small. At the higher dose of H_2O_2, the amount of hydroxyl radicals generated from the added H_2O_2 (Eq. (5)) most likely became so large that the amount of hydroxyl radicals generated by VUV irradiation of the water molecules (Eq. (3)) became negligibly small.

For the feasibility study, we calculated EE/O values for flow-through operation as follows (Bolton James et al., 2001):

$$EE/O = \frac{P}{F \cdot \log(c_0/c)} \quad (13)$$

where F is flow rate (m³/h). H_2O_2 was regarded as containing stored electric energy, which was added to the EE/O value: specifically, the calculation was conducted on the assumption that 1 kg of H_2O_2 was equivalent to 10 kWh (Müller and Jekel, 2001). The EE/O value decreased when H_2O_2 was added and continued to decrease as the H_2O_2 dose was increased (Table 4): VUV > VUV/H_2O_2 at 1 mg/L > UV/H_2O_2 at 1 mg/L > VUV/H_2O_2 at 5 mg/L ≈ UV/H_2O_2 at 5 mg/L. The calculated EE/O values for all the treatment processes, including VUV treatment, were <10, indicating the economic feasibility of the processes.

3.4. *Formation of by-products from NOM and inorganic ions*

3.4.1. *THMFP*

THMs in chlorinated drinking water are associated with increased cancer risk (Cantor et al., 1998). The WHO has established guideline values for four THM species: bromoform, DBCM, BDCM, and chloroform (100, 100, 60, and 200 μg/L, respectively). In the United States, individual THMs are not regulated, but total THMs (i.e., the sum of the concentrations of the above-mentioned 4 THMs) is regulated (annual average, 80 μg/L). In Japan, regulation values for bromoform, DBCM, BDCM, chloroform, and total THMs have been established at 90, 100, 30, 60, and 100 μg/L, respectively.

The THMFP of the raw lake water used in our experiments was 100 μg/L (Fig. 6(a)); chloroform and BDCM accounted for approximately 70% and 25%, respectively, of the total THMs produced. A small amount of DBCM was observed (approximately 5%), and no bromoform was detected. The chloroform concentration exceeded the Japanese Drinking Water Quality Standard (JDWQS). VUV treatment decreased THMFP by 22%. The hydrophobic fraction of NOM has been reported to show the greatest ability to produce CDBPs (Chang et al., 2001). Because VUV irradiation effectively decomposes the hydrophobic fraction of NOM (Buchanan et al., 2005), it is likely that the possible precursors of THMs were decomposed by VUV treatment, resulting in the observed decrease in THMFP. Buchanan et al. (2006) reported that THMFP increased with 32 J/cm² of VUV irradiation that was much higher than the VUV dose applied in the present study. These investigators presumed that the increase was due to the halogenation of low molecular weight compounds produced by the breakdown of large NOM compounds with the VUV irradiation. In contrast, in the present study, THMFP decreased with the VUV irradiation, of which dose was much lower than the dose applied in these investigators. The breakdown of large NOM compounds may not occur with the low VUV dose applied in the present study. The chloroform formation potential was decreased by VUV treatment, whereas the DBCM and BDCM formation potentials did not change. The precursors of chloroform in the raw lake water were likely decomposed to compounds that did not produce chloroform after chlorination, whereas the precursors of DBCM and BDCM may have been converted to compounds that did produce DBCM and BDCM after chlorination.

The chloroform formation potential was decreased further by both BAC and virgin GAC treatment; the removal percentages were 66% and 93%, respectively. The BDCM formation potential was not decreased by BAC treatment but was decreased by virgin GAC treatment. The DBCM formation potential was not decreased by either the BAC treatment or the virgin GAC treatment. Overall, BAC treatment decreased THMFP by 46%, and virgin GAC treatment reduced it by 81%, owing to the large reduction in the precursors of the predominant species (chloroform) by these treatment processes. Buchanan et al. (2008) reported that VUV/BAC treatment decreased THMFP, in agreement with our results. However, these investigators reported that the formation potentials of all THM species were decreased by the VUV/BAC treatment.

The THMFP of the groundwater was very low (2 μg/L, Fig. 6(b)), which we attributed to the low DOC concentration in the groundwater, and remained low (<8 μg/L) after the VUV, VUV/BAC, and VUV/GAC treatments.

3.4.2. *HAAFP*

HAAs are a public health concern owing to their potential genotoxicity and carcinogenicity (Richardson et al., 2007). We measured the formation potentials of 9 HAAs, including five species (BAA, CAA, DBAA, DCAA and TCAA) regulated under the designation HAA_5 by the United States Environmental Protection Agency (USEPA; 60 μg/L as an annual average), two species with established WHO guideline values (DCAA and TCAA; 50 and 200 μg/L, respectively), and three species listed

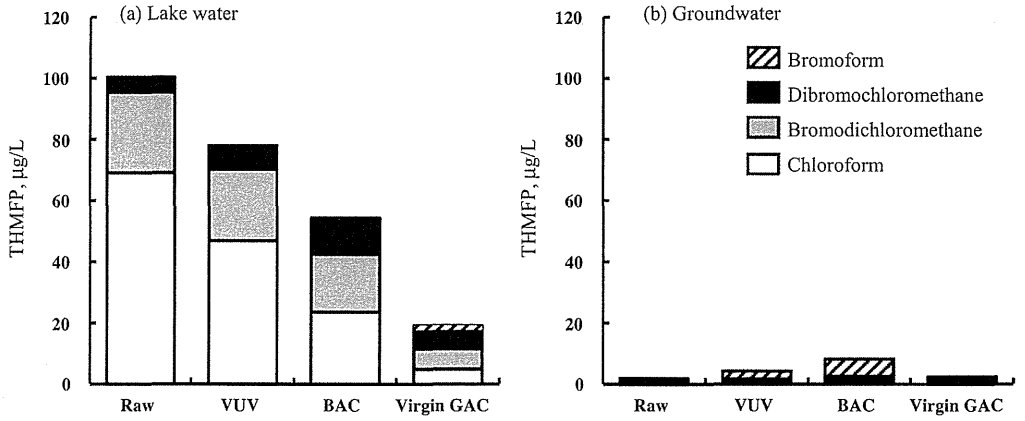

Fig. 6 – Changes in THMFPs in (a) lake water and (b) groundwater with VUV treatment (7.8 kJ/L) and subsequent treatment with BAC or virgin GAC. The values represent averages for two samples (6 measurements).

in the JDWQS (CAA, DCAA, and TCAA; 20, 40, and 200 μg/L, respectively).

Six of the nine HAAs (CAA, DBAA, BCAA, DCAA, TCAA, and BDCAA) were detected in the lake water samples after chlorination, whereas BAA, DBCAA, and TBAA were not detected (Fig. 7(a)). The HAAFP (i.e., the sum of the concentrations of the 9 HAAs after chlorination) of the raw lake water was approximately 80 μg/L. TCAA was present at the highest concentration (45 μg/L), followed by DCAA (23 μg/L). The concentrations of these compounds were under the JDWQS value. However, the HAA_5 value of the chlorinated lake water was 69 μg/L, which exceeded the USEPA regulation value. Unlike THMFP, HAAFP was not decreased by VUV treatment. Malliarou et al. (2005) have reported that the relationship between THMs and HAAs is site specific; in the present study, the precursors of the HAAs may have differed from those of the THMs. Buchanan et al. (2006) reported that HAAFP remains basically constant, with only small fluctuations, upon VUV irradiation at ≤ 32 J/cm^2 but decreases upon VUV irradiation at ≥ 48 J/cm^2. Our results at the lower VUV dose roughly agreed with theirs.

Precursors of HAAs in the VUV-treated lake water were effectively removed by the subsequent GAC treatment, reducing HAAFP. Buchanan et al. (2008) reported that HAAFP decreases with BAC treatment. We found that the HAA precursors could also be removed adsorptively even without the activity of microorganisms inhabiting the activated carbon. The BAC and virgin GAC treatments decreased HAAFP to 35 and 13 μg/L (23 and 7 μg/L as HAA_5), respectively, values that meet the USEPA HAA_5 standard. Finally, HAAFP was decreased by the GAC treatment, even though it did not decrease during VUV treatment at the VUV dose used in the present study.

The groundwater used in the present study did not produce any HAAs after chlorination (Fig. 7(b)). As was the case for THMs, the groundwater did not contain HAA precursors. After VUV treatment and subsequent GAC treatment, no HAAFP was observed likewise.

3.4.3. *Aldehydes*

Aldehydes are the main disinfection by-products of ozonation (Cancho et al., 2002), but aldehydes are also reportedly produced by chlorination (Kransner et al., 1989). Formaldehyde has been reported to be mutagenic (Lewis and Chestner, 1981) and is classified as a human carcinogen (Group A) by the International Agency for Research on Cancer. Various other aldehydes have also been reported to be mutagenic (Brambilla et al., 1989); in particular, glyoxal is reportedly more mutagenic than formaldehyde (Marnett et al., 1985). Among the 10 aldehydes measured in the present study, formaldehyde is the only one with regulated values for drinking water: 80 and 900 μg/L in the JDWQS and the WHO guidelines, respectively. In the present study, four of the ten aldehydes (formaldehyde, propanal, butanal, and glyoxal) were detected in the chlorinated samples.

The raw lake water used in the experiments contained no aldehydes (data not shown), whereas after chlorination, the water contained some aldehydes (Fig. 8(a)), which were

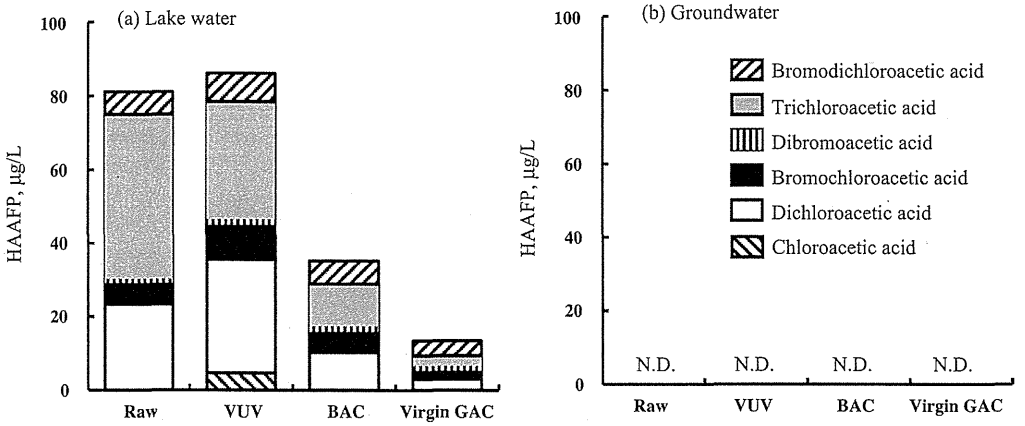

Fig. 7 – Changes in HAAFPs in (a) lake water and (b) groundwater with VUV treatment (7.8 kJ/L) and subsequent treatments with BAC or virgin GAC. The values represent averages for 2 samples (6 measurements).

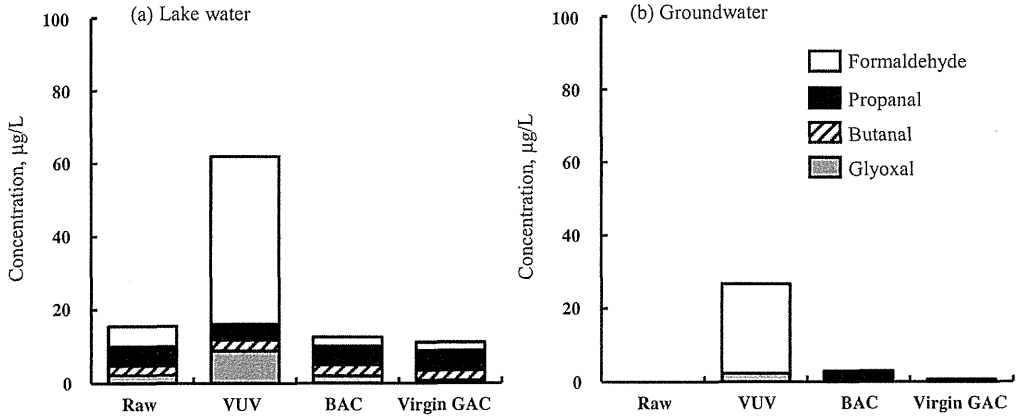

Fig. 8 – Changes in aldehyde concentrations after chlorination of (a) lake water and (b) groundwater with VUV treatment (7.8 kJ/L) and subsequent treatments with BAC or virgin GAC. The values represent averages for two samples (six measurements).

produced by the reaction of chlorine with NOM (Becher et al., 1992) present in the raw water. After VUV treatment followed by Cl_2 treatment (VUV/Cl_2), a relatively high concentration (approximately 40 μg/L) of formaldehyde was observed. Thomson et al. (2004) reported that formaldehyde was the dominant species among low molecular weight carbonyl compounds present in a VUV-irradiated surface water, which agrees with our results. Zhang et al. (2008) reported that aldehydes are produced from NOM during a catalytic ozonation process, in which hydroxyl radicals play a critical role, and that among the aldehydes, formaldehyde was produced in the largest amounts. During VUV treatment in the present study, most of the reactions that occurred were caused by hydroxyl radicals, and this is likely the reason that a large amount of formaldehyde was produced. Additionally, some of the NOM that was not converted to formaldehyde during chlorination may have been transformed to formaldehyde-forming compounds during VUV treatment, and therefore would also contribute to the increase in the formaldehyde concentration after chlorination. Glyoxal was also observed in the lake water subjected to VUV/Cl_2 treatment, and this result agrees with previous results reported by (Zhang et al., 2008). However, when the VUV-treated lake water was subsequently treated with BAC or virgin GAC, the formaldehyde and glyoxal concentrations observed after the final chlorination were substantially lower than before the carbon treatment. This decrease may have been due to biological or adsorptive removal of aldehyde-forming precursors, aldehydes produced by VUV treatment, or both. In summary, aldehydes were produced during VUV treatment but their concentrations could be reduced by subsequent treatment with BAC or GAC. These results clearly indicate that VUV treatment should be used in combination with BAC or GAC treatment for optimum removal of disinfection by-products.

The raw groundwater contained no aldehydes (data not shown), and no aldehydes were detected even after chlorination (Fig. 8(b)), indicating that aldehyde-forming precursors were probably not present in the raw groundwater. However, formaldehyde was observed in the chlorinated VUV-treated groundwater, which indicates that some of the organic matter in the raw groundwater was transformed into either formaldehyde or formaldehyde precursors by VUV treatment. The formaldehyde precursors and formaldehyde itself were effectively removed by both BAC and virgin GAC, in agreement with the results observed with the lake water. Only a small amount of aldehydes was detected after the BAC and GAC treatments.

3.4.4. *Nitrite*

Nitrite is formed by the reaction of nitrate with solvated electrons and hydrogen atoms that are formed by VUV photolysis of water (Zoschke et al., 2014); nitrite formation should be taken into account in real-world applications of VUV irradiation. Nitrite was produced by VUV irradiation of the raw lake water (Fig. 9(a)), but the concentration was very low (0.2 mg-N/L) because the nitrate concentration of the raw lake water was also very low. In contrast, the nitrite concentration produced by VUV irradiation of the raw groundwater was 1.3 mg-N/L (Fig. 9(b)), which exceeds the USEPA maximum contaminant level (1 mg-N/L) and the European drinking water standard (0.1 mg-N/L). The nitrite was not removed by subsequent treatment with virgin GAC. However, subsequent BAC treatment completely removed the nitrite. Nitrifying bacteria in the GAC most likely oxidized the nitrite to nitrate. For nitrite removal, BAC treatment is recommended after VUV irradiation.

3.4.5. *Bromate*

To investigate bromate production from bromide, we prepared buffered DTW spiked with bromide at a high concentration (100 μg-Br/L), and we then conducted decomposition experiments using the VUV, VUV/TiO_2, UV, and UV/TiO_2 treatments (10.8 kJ/L). After all the treatments, the bromate concentrations (<0.1 μg-BrO_3^-/L) were well below the WHO guideline value, the USEPA maximum contaminant level, and the JDWQS value (10 μg-BrO_3^-/L) (data not shown). Several methods for suppressing bromate production during ozonation have been reported (Pinkernell and von Gunten, 2001), but in actual practice, the difficulty in keeping certain operation parameters in a suitable range may limit the application of the ozonation process. In contrast, the VUV, VUV/H_2O_2, and UV/H_2O_2 treatments minimized the formation of bromate even when the raw water was contaminated with a high concentration of bromide.

To minimize by-product formation during VUV treatment, subsequent treatment with GAC or BAC is recommended. The efficiency of 1,4-dioxane decomposition by VUV treatment was lower than the efficiencies by the other AOPs. However, VUV treatment is operationally simple and requires no

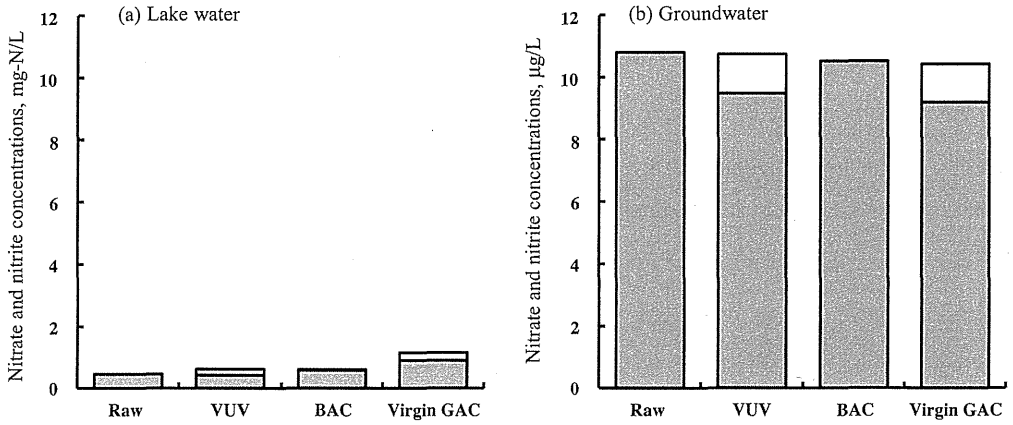

Fig. 9 – Change in nitrate (gray) and nitrite (white) concentrations in (a) lake water and (b) groundwater with VUV treatment (7.8 kJ/L) and subsequent treatments with BAC or virgin GAC. The values represent averages for two samples (six measurements).

chemicals. VUV treatment was revealed to effectively decompose 1,4-dioxane with economic feasibility, and by-product formation could be suppressed by subsequent GAC or BAC treatment. Thomson et al. (2002) reported that the EE/O values for the VUV treatment on NOM removal were approximately 80 (based on OD_{254}) and 200 (based on DOC) kWh/(m^3·order), respectively, and they were still >20 kWh/(m^3·order) even with 50 mg/L of hydrogen peroxide addition. These values were much larger than the values (<1 kWh/(m^3·order)) obtained in the present study for 1,4-dioxane removal, and regarded to be economically infeasible under the EE/O criterion (feasible when EE/O < 10). Accordingly, not NOM but persistent compounds, such as 1,4-dioxane, that are quite difficult to be removed by other treatment methods are recommended to be included in main targets of the VUV treatment.

4. Conclusions

1. For the first time, VUV treatment was used to decompose 1,4,-dioxane, a persistent organic compound, in water, and the treatment was found to be economically feasible. The rate of 1,4-dioxane decomposition for the treatments increased in the order UV < UV/TiO_2 < VUV < VUV/TiO_2. The rate constant for 1,4-dioxane decomposition was smaller than the rate constants for 2-MIB and geosmin decomposition in all of the tested treatments.
2. Addition of H_2O_2 accelerated the decomposition of 1,4-dioxane during both UV and VUV treatments. VUV/H_2O_2 treatment was superior to UV/H_2O_2 treatment at a small H_2O_2 dose, but the decomposition efficiencies of the two treatments were almost the same at a large H_2O_2 dose.
3. VUV treatment slightly decreased THMFP but had no effect on HAAFP, whereas the treatment increased the total aldehyde concentration. However, THMFP, HAAFP, and aldehyde concentration could be reduced by subsequent GAC treatment. Although nitrite was produced during VUV treatment, it completely disappeared after subsequent BAC treatment. VUV treatment should be used in combination with BAC or GAC treatment to minimize by-product formation. Even though the raw water contained a high concentration of bromide (100 μg-Br/L), no bromate (<0.1 μg-BrO_3^-/L) was produced by VUV treatment.
4. The combination of VUV and BAC or GAC treatments is simple and requires no chemicals, and it effectively and economically removed 1,4-dioxane with limited by-product formation.

Acknowledgements

This research was supported in part by a Grant-in-Aid for Scientific Research (S) (24226012), Health and Labor Sciences Research Grant (Research on Health Security Control), and by Bureau of Waterworks, Tokyo Metropolitan Government.

References

Abe, A., 1999. Distribution of 1,4-dioxane in relation to possible sources in the water environment. Sci. Total Environ. 227, 41–47.

Adams, C.D., Scanlan, P.A., Secrist, N.D., 1994. Oxidation and biodegradability enhancement of 1,4-dioxane using hydrogen peroxide and ozone. Environ. Sci. Technol. 28, 1812–1818.

Afzal, A., Oppenländer, T., Bolton, J.R., El-Din, M.G., 2010. Anatoxin-a degradation by advanced oxidation processes: vacuum-UV at 172 nm, photolysis using medium pressure UV and UV/H2O2. Water Res. 44, 278–286.

Andrews, S., Huck, P., Chute, A., Bolton, J., Anderson, W., 1995. UV oxidation for drinking water-feasibility studies for addressing specific water quality issues. AWWA Annu. Conf., 1881–1898.

Becher, G., Ovrum, N.M., Christman, R.F., 1992. Novel chlorination by-products of aquatic humic substances. Sci. Total Environ. 117–118, 509–520.

Black, D.B., Lawrence, R.C., Lovering, B.G., Watson, J.R., 1983. Gas-liquid chromatographic method for determining 1,4-dioxane in cosmetics. J. Assoc. Off. Anal. Chem. 66, 180–183.

Bolton James, R., Bircher Keith, G., Tumas, W., Tolman Chadwick, A., 2001. Figures-of-merit for the technical development and application of advanced oxidation technologies for both electric- and solar-driven systems (IUPAC Technical Report). Pure Appl. Chem., 627.

Brambilla, G., Cajelli, E., Canonero, R., Martelli, A., Marinari, U.M., 1989. Mutagenicity in V79 Chinese hamster cells of n-alkanals produced by lipid peroxidation. Mutagenesis 4, 277–279.

Buchanan, W., Roddick, F., Porter, N., 2006. Formation of hazardous by-products resulting from the irradiation of natural organic matter: comparison between UV and VUV irradiation. Chemosphere 63, 1130–1141.

Buchanan, W., Roddick, F., Porter, N., 2008. Removal of VUV pre-treated natural organic matter by biologically activated carbon columns. Water Res. 42, 3335–3342.

Buchanan, W., Roddick, F., Porter, N., Drikas, M., 2005. Fractionation of UV and VUV pretreated natural organic matter from drinking water. Environ. Sci. Technol. 39, 4647–4654.

Cancho, B., Ventura, F., Galceran, M.T., 2002. Determination of aldehydes in drinking water using pentafluorobenzylhydroxylamine derivatization and solid-phase microextraction. J. Chromatogr. A 943, 1–13.

Cantor, K.P., Lynch, C.F., Hildesheim, M., Dosemeci, M., Lubin, J., Alavanja, M., Craun, G., 1998. Drinking water source and chlorination byproducts I. Risk of bladder cancer. Epidemiology 9, 21–28.

Chang, E.E., Chiang, P.-C., Ko, Y.-W., Lan, W.-H., 2001. Characteristics of organic precursors and their relationship with disinfection by-products. Chemosphere 44, 1231–1236.

Coleman, H.M., Vimonses, V., Leslie, G., Amal, R., 2007. Degradation of 1,4-dioxane in water using TiO_2 based photocatalytic and H2O2/UV processes. J. Hazard. Mater. 146, 496–501.

Fuh, C.B., Lai, M., Tsai, H.Y., Chang, C.M., 2005. Impurity analysis of 1,4-dioxane in nonionic surfactants and cosmetics using headspace solid-phase microextraction coupled with gas chromatography and gas chromatography–mass spectrometry. J. Chromatogr. A 1071, 141–145.

Gaya, U.I., Abdullah, A.H., 2008. Heterogeneous photocatalytic degradation of organic contaminants over titanium dioxide: a review of fundamentals, progress and problems. J. Photochem. Photobiol. C: Photochem. Rev. 9, 1–12.

Glaze, W.H., Peyton, G.R., Lin, S., Huang, R.Y., Burleson, J.L., 1982. Destruction of pollutants in water with ozone in combination with ultraviolet radiation. II. Natural trihalomethane precursors. Environ. Sci. Technol. 16, 454–458.

Glaze, W.H., Schep, R., Chauncey, W., Ruth, E.C., Zarnoch, J.J., Aieta, E.M., Tate, C.H., McGuire, M.J., 1990. Evaluation oxidants for the removal of model taste and odour compounds from a municipal water supply. J. Am. Waterworks Assoc. 85, 79–84.

Guo, W., Brodowsky, H., 2000. Determination of the trace 1,4-dioxane. Microchem. J. 64, 173–179.

Hebert, A., Forestier, D., Lenes, D., Benanou, D., Jacob, S., Arfi, C., Lambolez, L., Levi, Y., 2010. Innovative method for prioritizing emerging disinfection by-products (DBPs) in drinking water on the basis of their potential impact on public health. Water Res. 44, 3147–3165.

Hill, R.R., Jeffs, G.E., Roberts, D.R., 1997. Photocatalytic degradation of 1 4-dioxane in aqueous solution. J. Photochem. Photobiol. A: Chem. 108, 55–58.

Imoberdorf, G., Mohseni, M., 2012. Kinetic study and modeling of the vacuum-UV photoinduced degradation of 2,4-D. Chem. Eng. J. 187, 114–122.

Isaacson, C., Mohr, T.K.G., Field, J.A., 2006. Quantitative determination of 1,4-dioxane and tetrahydrofuran in groundwater by solid phase extraction GC/MS/MS‡. Environ. Sci. Technol. 40, 7305–7311.

Ishikawa, T., Yamaoka, H., Harada, Y., Fujii, T., Nagasawa, T., 2002. A general process for in situ formation of functional surface layers on ceramics. Nature 416, 64–67.

Joyner, R.A., 1912. Die Affinitätskonstante des Hydroperoxyds. Zeitschrift für anorganische Chemie 77, 103–115.

JWWA, 2011. Standard Methods for the Examination of Water. Jpn. Water Works Assoc.

Klečka, G.M., Gonsior, S.J., 1986. Removal of 1,4-dioxane from wastewater. J. Hazard. Mater. 13, 161–168.

Kransner, S.W., McGuire, M.J., Jacangelo, J.G., Patania, N.L., Reagan, K.M., Aieta, E.M., 1989. The occurrence of disinfection by-products in US drinking water. J. Am. Water Works Assoc. 81, 41–53.

Kruithof, J.C., Kamp, P.C., Martijn, B.J., 2007. UV/H_2O_2 treatment: a practical solution for organic contaminant control and primary disinfection. Ozone: Sci. Eng. 29, 273–280.

Kutschera, K., Börnick, H., Worch, E., 2009. Photoinitiated oxidation of geosmin and 2-methylisoborneol by irradiation with 254 nm and 185 nm UV light. Water Res. 43, 2224–2232.

LaVerne, J.A., 1989. The production of oh radicals in the radiolysis of water with 4He ions. Radiat. Res. 118, 201–210.

Lawton, L.A., Robertson, P.K.J., Robertson, R.F., Bruce, F.G., 2003. The destruction of 2-methylisoborneol and geosmin using titanium dioxide photocatalysis. Appl. Catal. B: Environ. 44, 9–13.

Lesage, S., Jackson, R.E., Priddle, M.W., Riemann, P.G., 1990. Occurrence and fate of organic solvent residues in anoxic groundwater at the Gloucester landfill. Can. Environ. Sci. Technol. 24, 559–566.

Lewis, B., Chestner, S., 1981. Formaldehyde in dentistry: a review of mutagenic and carcinogenic potential. J. Am. Dental Assoc. 103, 429–434.

Liao, C.-H., Gurol, M.D., 1995. Chemical oxidation by photolytic secomposition of hydrogen peroxide. Environ. Sci. Technol. 29, 3007–3014.

Lopez, A., Bozzi, A., Mascolo, G., Kiwi, J., 2003. Kinetic investigation on UV and UV/H2O2 degradations of pharmaceutical intermediates in aqueous solution. J. Photochem. Photobiol. A: Chem. 156, 121–126.

Müller, J.-P., Jekel, M., 2001. Comparison of advanced oxidation processes in flow-through pilot plants (Part I). Water Sci. Technol. 44, 303–309.

Malliarou, E., Collins, C., Graham, N., Nieuwenhuijsen, M.J., 2005. Haloacetic acids in drinking water in the United Kingdom. Water Res. 39, 2722–2730.

Marnett, L.J., Hurd, H.K., Hollstein, M.C., Levin, D.E., Esterbauer, H., Ames, B.N., 1985. Naturally occurring carbonyl compounds are mutagens Salmonella tester strain TA104. Mutat. Res./Fund. Mol. Mech. Mutagen. 148, 25–34.

Maurino, V., Calza, P., Minero, C., Pelizzetti, E., Vincenti, M., 1997. Light-assisted 1,4-dioxane degradation. Chemosphere 35, 2675–2688.

McGuire, M.J., Suffet, I.H., Radziul, J.V., 1978. Assessment of unit processes for the removal of trace organic compounds from drinking water. J. Am Water Works Assoc. 10, 565–572.

Mehrvar, M., Anderson, W.A., Moo-Young, M., 2000. Photocatalytic degradation of aqueous tetrahydrofuran, 1,4-dioxane, and their mixture with TiO_2. Int. J. Photoenergy 2, 67–80.

Mehrvar, M., Anderson, W.A., Moo-Young, M., 2002. Comparison of the photoactivities of two commercial titanium dioxide powders in the degradation of 1,4-dioxane. Int. J. Photoenergy 4, 141–146.

Oppenländer, T., 2007. Mercury-free sources of VUV/UV radiation: application of modern excimer lamps (excilamps) for water and air treatment. J. Environ. Eng. Sci. 6, 253–264.

Oppenländer, T., Sosnin, E., 2005. Mercury-free vacuum-(VUV) and UV excilamps: lamps of the future? IUVA News 7, 16–20.

Pinkernell, U., von Gunten, U., 2001. Bromate minimization during ozonation: mechanistic considerations. Environ. Sci. Technol. 35, 2525–2531.

Richardson, S.D., Plewa, M.J., Wagner, E.D., Schoeny, R., DeMarini, D.M., 2007. Occurrence, genotoxicity, and carcinogenicity of regulated and emerging disinfection by-products in drinking water: a review and roadmap for research. Mutat. Res./Rev. Mutat. Res. 636, 178–242.

Rosenfeldt, E.J., Melcher, B., Linden, K.G., 2005. UV and UV/H_2O_2 treatment of methylisoborneol (MIB) and geosmin in water. J. Water Supply: Res. Technol. – AQUA 54, 423–434.

Stefan, M.I., Bolton, J.R., 1998. Mechanism of the degradation of 1,4-dioxane in dilute aqueous solution using the UV/hydrogen peroxide process. Environ. Sci. Technol. 32, 1588–1595.

Suh, J.H., Mohseni, M., 2004. A study on the relationship between biodegradability enhancement and oxidation of 1,4-dioxane using ozone and hydrogen peroxide. Water Res. 38, 2596–2604.

Szabó, R.K., Megyeri, C., Illés, E., Gajda-Schrantz, K., Mazellier, P., Dombi, A., 2011. Phototransformation of ibuprofen and ketoprofen in aqueous solutions. Chemosphere 84, 1658–1663.

Tanabe, A., Kawata, K., 2008. Determination of 1,4-dioxane in household detergents and cleaners. J. AOAC Int. 91, 439–444.

Tanabe, A., Tsuchida, Y., Ibaraki, T., Kawata, K., 2006. Impact of 1,4-dioxane from domestic effluent on the agano and shinano rivers, Japan. Bull. Environ. Contam. Toxicol. 76, 44–51.

Thomson, J., Roddick, F., Drikas, M., 2002. Natural organic matter removal by enhanced photooxidation using low pressure mercury vapour lamps. Water Sci. Technol. 2 (5–6), 435–443.

Thomson, J., Roddick, F.A., Drikas, M., 2004. Vacuum ultraviolet irradiation for natural organic matter removal. J. Water Supply: Res. Technol. – AQUA 53, 193–206.

Weeks, J.L., Gordon, S., 1963. Absorption coefficients of liquid water and aqueous solutions in the far ultraviolet. Radiat. Res. 19, 559–567.

Zenker, M.J., Borden, R.C., Barlaz, M.A., 2003. Occurrence and treatment of 1,4-dioxane in aqueous environments. Environ. Eng. Sci. 20, 423–432.

Zhang, T., Lu, J., Ma, J., Qiang, Z., 2008. Comparative study of ozonation and synthetic goethite-catalyzed ozonation of individual NOM fractions isolated and fractionated from a filtered river water. Water Res. 42, 1563–1570.

Zoschke, K., Börnick, H., Worch, E., 2014. Vacuum-UV radiation at 185 nm in water treatment – a review. Water Res. 52, 131–145.

Zoschke, K., Dietrich, N., Börnick, H., Worch, E., 2012. UV-based advanced oxidation processes for the treatment of odour compounds: efficiency and by-product formation. Water Res. 46, 5365–5373.

Journal of Membrane Science 477 (2015) 115–122

Contents lists available at ScienceDirect

Journal of Membrane Science

journal homepage: www.elsevier.com/locate/memsci

Hydraulically irreversible membrane fouling during coagulation–microfiltration and its control by using high-basicity polyaluminum chloride

Masaoki Kimura [a], Yoshihiko Matsui [b,*], Shun Saito [a], Tomoya Takahashi [a], Midori Nakagawa [a], Nobutaka Shirasaki [b], Taku Matsushita [b]

[a] Graduate School of Engineering, Hokkaido University, N13W8, Sapporo 060-8628, Japan
[b] Faculty of Engineering, Hokkaido University, N13W8, Sapporo 060-8628, Japan

ARTICLE INFO

Article history:
Received 30 October 2014
Received in revised form
21 December 2014
Accepted 22 December 2014
Available online 2 January 2015

Keywords:
Ceramic
Foulant
Silicate
Coagulant
Basicity

ABSTRACT

The extent of hydraulically irreversible membrane fouling in a coagulation–filtration system depends on several factors, including properties of the coagulant. Effects of polyaluminum chloride (PACl) coagulant properties, specifically basicity and sulfation, were investigated by conducting long-term direct filtration experiments. Elemental analysis determined Al and Si to be the major foulants, though the Si/Al ratios of the foulants differed from those of coagulated floc particles. While floc particle size depended on the concentrations of sulfate ions and polymeric species in the PACls, floc-size changes did not affect transmembrane pressure (TMP) buildup and thus did not affect irreversible fouling. Differences in PACl basicity, which affected the distribution of aluminum species, resulted in changes to the degree of irreversible fouling.

Pretreatment with high-basicity (71%) PACl was superior to pretreatment with normal-basicity (51%) PACl in reducing irreversible fouling and attenuating TMP buildup during filtration. Higher basicities resulted in less Al breakthrough and a decrease in the Si/Al ratio of the foulants. However, TMP buildup was the same for PACls with basicities of 71% and 90%; therefore, TMP buildup is not simply related to Al breakthrough and deposition. Increasing the basicity of PACls would be an effective way to reduce the amount of foulant deposited on the membrane by decreasing the amount of aluminum that passes through the membrane.

1. Introduction

Coagulation, adsorption, and oxidation are widely used as pretreatment processes for microfiltration (MF) in water purification to alleviate membrane fouling and enhance the removals of micropollutants and disinfection byproduct precursors [1]. In MF with ceramic membranes, coagulation–flocculation with polyaluminum chloride (PACl) is a successful pretreatment for removing soluble substances and reducing the decrease in membrane permeability during long-time operation [2]. This process is commonly used in full-scale water treatment. Coagulation pretreatment destabilizes and agglomerates the colloidal and particulate foulants, increasing their size and thereby mitigating pore constriction and blockage and the formation of a porous cake layer. Additionally, increased particle size reduces the specific cake resistance, according to the Carman–Kozeny relationship, and thus increases permeability. However, membrane fouling is not completely avoided since aquatic colloids are not removed, which cause fouling by narrowing or blocking membrane pores, and substances retained on the membrane that form a gel or cake layer still contribute resistance.

The permeability of the cake layer formed from floc particles during coagulation has been extensively studied for dependence on floc size, strength, and fractal structure [3–5]. Coagulated flocs with a high fractal dimension have low compressibility, leading to low membrane permeability [6]. Other studies, however, found high compressibility in flocs related to a higher specific resistance of the cake layer [7,8]. Coagulated flocs with a high fractal dimension formed by PACl have a more compact structure than flocs formed by alum [9]. Therefore, the MF membrane permeability deteriorates more severely during PACl coagulation than during alum coagulation due to the higher specific resistance of the cake layer. Liu et al. [10], in contrast, report that floc particles of a high fractal dimension as well as a large size formed by two-stage coagulant dosing mitigated TMP development more than those formed by a single dose. The strength (resistance toward shear stress) of floc particles formed by coagulation also plays an important role in the permeability of the cake layer

* Corresponding author. Tel./Fax: +81 11 706 7280.
E-mail address: matsui@eng.hokudai.ac.jp (Y. Matsui).

http://dx.doi.org/10.1016/j.memsci.2014.12.033
0376-7388/

[11–13]. The increase in transmembrane pressure (TMP) in an ultrafiltration (UF) system is lower with floc breakage, which lowers the fractal dimension of flocs, than without breakage [14]. Xu and Gao [3], however, reported that an increased shear for floc breakage considerably decreased the floc size and increased the floc compactness, thus increasing resistance and lowering the permeability of the cake layer. Therefore, an increase in floc strength could enhance the permeability of the cake layer [4]. Overall, findings on the relationship of floc characteristics to membrane performance are not consistent, though it is clear the structure of the cake layer plays an important role in membrane permeability.

In a ceramic membrane MF system, the permeability of the cake layer may not be a crucial issue, because an integrated, intensive, hydraulic backwash process would eject most of the cake layer. After coagulation, the affinity of the membrane for destabilized contaminants and their aggregates is lower than without coagulation, which leads to a more effective backwash. Hence, with an integrated, hydraulic backwash, the degree of fouling from cake layer formation would be minimized. Hydraulically irreversible fouling is the main concern in full-scale membrane filtration facilities because it determines energy consumption for long-term membrane filtration and affects the sustainable operation of the facility. Irreversible fouling is caused by contaminants that do not react with or adsorb to hydrolytic species formed by the coagulant and thus are not destabilized [15]. Many studies have been conducted to better understand the behavior of membrane foulants and elucidate fouling mechanisms, but these studies have seldom identified practical solutions to the membrane-fouling problem.

A limited amount of research has concerned the extent to which different coagulant types might be exploited to most effectively reduce the extent of irreversible fouling. Tran et al. [16] reported that polysilicato-iron coagulants were better at mitigating irreversible fouling than aluminum-based coagulants at a higher dose while aluminum-based coagulants worked better at a lower dose. Their study suggests that the effect on membrane fouling is a complex phenomenon where many factors including the residual DOC and the property of small-size flocs influence the fouling to various extents. Membrane fouling may also be caused by hydrolytic species of coagulants, though it has not been fully studied [1]. The key consideration is that coagulant characteristics required for membrane pretreatment are not necessarily the same as those for coagulation and settling. Conventional coagulation is designed to form large-size floc particles that settle out, whereas, for membrane pretreatment, coagulation should allow for direct filtration of floc that results in improved filtrate water quality and alleviates membrane fouling.

In this study, we investigated five PACl coagulants suitable for direct MF. The effect of PACl properties (basicity and sulfated/nonsulfated) on hydraulically irreversible membrane fouling (hereafter called irreversible fouling), which results in a long-term TMP rise, was studied, in particular, by focusing on the residual aluminum concentration in filtrates and aluminum deposits on membranes.

2. Materials and methods

2.1. Coagulants

Four PACls were obtained from the Taki Chemical Co. (Kakogawa, Japan): conventional normal-basicity (51%) sulfated PACl (designated as PACl-51s), high-basicity (71%) sulfated PACl (PACl-71s), high-basicity (71%) nonsulfated PACl (PACl-71), and very-high-basicity (90%) nonsulfated PACl (PACl-90). A second very-high-basicity (90%) nonsulfated PACl (PACl-90b) was prepared in the authors' laboratory by the base titration method using NaOH (0.3 M) and $AlCl_3$ (0.5 M) [17]. The distributions of aluminum species in the coagulants were determined by the ferron method [17]. These species were assumed to be monomeric, polymeric, and colloidal aluminum species on the basis of their reaction rates with ferron reagent (8-hydroxy-7-iodo-5-quinolinesulfonic acid; Wako Pure Chemical Industries, Osaka, Japan), denoted Ala, Alb, and Alc, respectively [18]. Ala denotes aluminum species that reacted with ferron instantaneously (within 30 s); Alb denotes species that reacted with ferron within 120 min; and Alc denotes species that did not react. Properties of the PACls are listed in Table 1S (Supplementary data).

2.2. Pilot-scale MF system

Experiments were conducted with the coagulation-direct MF pilot plant at the Water Quality Center of the Sapporo Waterworks Bureau, Japan. The plant has two parallel lines (Lines A and B) with the same

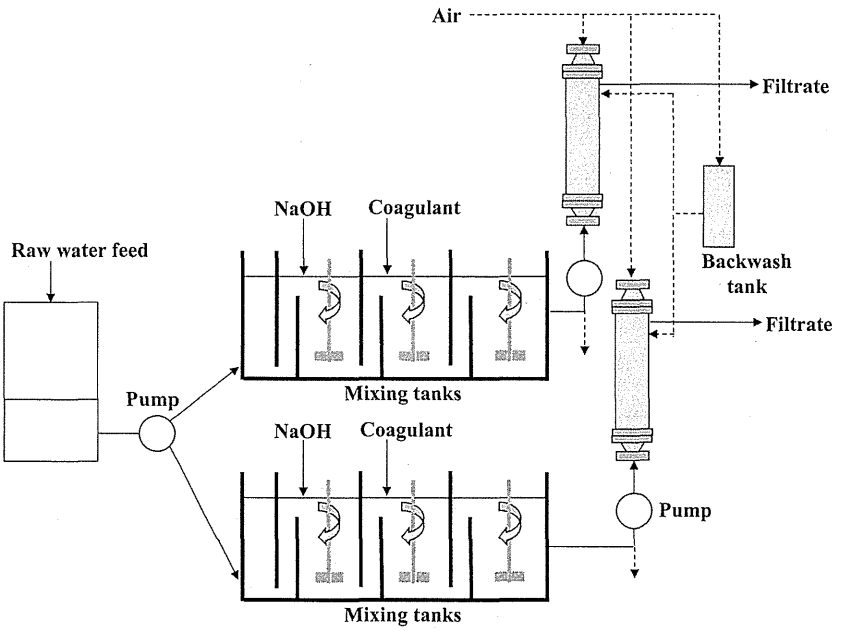

Fig. 1. Pilot-scale MF systems.

configuration, each consisting of coagulation mixing tanks, a feed pump, a membrane module, and a hydraulic backwash unit in series (Fig. 1). The two lines were operated in parallel under identical conditions except for coagulant type and dosage of caustic soda for pH control, which enabled direct comparison of the experiments. The coagulation process was performed in rapidly and slowly stirred mixing tanks with detention times of 7.3 and 12.5 min, respectively. Mixing intensities were 60 rpm (G=68.5 s^{-1}) and 20 rpm (G=13.3 s^{-1}) unless otherwise noted. Each line has a small membrane module containing a tubular, ceramic monolith membrane element (nominal pore size, 0.1 μm; 55 channels; diameter, 3 cm; length, 10 cm; effective filtration area, 0.043 m^2; Metawater Co., Tokyo, Japan). The element was specially designed for small-scale experiments; in comparison, the membrane element used for the full-scale filtration plant has a membrane surface area of 25 m^2, a diameter of 1800 mm, and a length of 1.5 m. Before each filtration run, the membrane element was chemically-cleaned and, after housing the module, the initial permeability was checked. The module was configured for dead-end filtration with constant flow to the membrane module (filtration rate, 0.125 m/h) by positive pressure. The membranes were hydraulically backwashed every hour from the filtrate side with membrane permeate at a pressure of 500 kPa for 20 s, and the retentate was ejected by pressurized water and air. Feed pressure, raw water turbidity, water temperature, and coagulation pH were monitored continuously, and the data were stored. Coagulant dose was automatically adjusted as a function of raw water turbidity [dosage/(mg-Al/L)=1.06 for 0–7 NTU, dosage/(mg-Al/L)=0.151 × turbidity/NTU for 7–14 NTU, dosage/(mg-Al/L)=0.034 × turbidity/NTU+1.65 for 14–140 NTU; these formulas were determined from the PACl dosage–turbidity relationship obtained at the Moiwa Water Treatment Plant, which treats the same raw water]. Coagulation pH was controlled at a constant value by the automatic dosage of caustic soda, except for the first set of runs (Run 1). Plant operation was continued either for 25–35 days or until the TMP reached about 100 kPa. In some cases, operation was terminated due to cessation of raw water flow from the Water Quality Center. During plant operation, samples of coagulated waters before direct MF were taken manually and immediately filtered through organic membranes (polycarbonate, Isopore, Millipore Corp.) of the same nominal pore size, 0.1 μm, as that of the ceramic membrane. For some runs, samples were filtered through organic membranes of various molecular mass cutoffs (500 Da, cellulose acetate, Amicon-Y, Millipore Corp; 1, 3, 10, and 100 kDa, regenerated cellulose, Ultracell-PL, Millipore Corp.). In total, 11 runs of parallel filtrations were conducted (Table 2S, Supplementary data). Additionally, for supplementary membrane filtrate sampling and foulant analysis, seven pairs of runs were carried out with PACl-60s (sulfated, basicity 60%, Taki Chemical Co.), PACl-65s (sulfated, basicity 65%, Taki Chemical Co.) and PACl-85 (nonsulfated, basicity 85%, Taki Chemical Co.).

2.3. Water quality

The plant treated Toyohira River water that was taken at Moiwa Dam (42.966182N, 141.269428E) and transported to the Water Quality Center through pipelines. The concentrations of dissolved organic carbon (DOC) and aluminum in the water were determined by the UV/persulfate oxidation method (Sievers 900 TOC Analyzer, GE Analytical Instruments, Boulder, CO, USA) and inductively coupled plasma mass spectrometry (ICP-MS, HP-7700, Agilent Technologies, Inc., Santa Clara, CA, USA), respectively. The characteristics of the raw water and the coagulation pH are listed in Table 2S (supplementary data).

2.4. Chemical cleaning of membrane and foulant analysis

After the final hydraulic backwashing in a filtration run, the membrane element was removed from the module and chemically cleaned by repeating the following soak cycle three times: sulfuric acid (0.02 N) for 18 h, Milli-Q water (Millipore Corp.) for 1 min, sodium hypochlorite (1500 mg-Cl_2/L) for 18 h, and Milli-Q water for 1 min. The spent cleaning solutions and Milli-Q waters were analyzed for organic C (Shimadzu TOC-5000A, Kyoto, Japan), Al, Si, Fe, Mn, and Ca (ICP-MS, HP-7700, Agilent Technologies, Inc.) to determine the concentrations of membrane foulants. Al and Si elemental analyses were conducted on the floc particles retained on the organic membrane filter from the manually collected and filtered samples (PTFE, 0.1 μm, Omnipore, Millipore Corp.) and on the ceramic membrane retentates ejected in the hydraulic backwash process.

3. Results and discussion

3.1. Effect of high-basicity (71%) PACl

Five pairs of runs (parallel filtrations) were conducted with PACl-71s in one line and PACl-51s in the other line. The rates of TMP buildup over the period of operation were lower when feedwater was pretreated with PACl-71s than with PACl-51s (Fig. 2). Even at pH 7.5, which sees more membrane fouling, PACl-71s lowered the rate of TMP buildup (Fig. 2C). Additional runs in which coagulation was conducted at pH 7.0 and pH 7.1 showed similar results, with the TMP following PACl-71s coagulation remaining at a low level throughout the period of operation (Fig. 1S, Supplementary data). The consistent results in the five pairs of runs indicate that the difference in the TMP buildups between PACl-71s and PACl-51s was not due to any very slight difference in initial membrane permeability. Moreover, PACl-71s was used in Line B in Runs 1, 2, and 3 and in Line A in Runs 4 and 5. Therefore, the difference in TMP rise is not due to any inherent characteristics of the line, including the membrane element used. We interpret the low rate of TMP buildup in the filtration with periodic backwash as mild irreversible fouling. The high rate of TMP buildup is characterized as severe irreversible fouling. Floc particle size is a key characteristic that affects reversible fouling, but may not be related to irreversible fouling. Fine floc particles were more often observed in the mixing tank after the addition of PACl-71s than after the addition of PACl-51s (Fig. 2S, Supplementary data), but addition of PACl-71s yielded a lower rate of TMP rise. The effects of floc particle size are further explored in Section 3.3.

The masses of Al and other elements extracted from the fouled membrane by chemical cleaning are shown in Fig. 3. The amounts of Al and Si were the largest among the elements extracted, followed by organic C and Ca, suggesting that the irreversible foulants were mainly composed of these elements. The low relative loadings of organic C indicate natural organic matter (NOM) was not a main cause of membrane fouling: this might be due to the low DOC concentrations in the raw waters (Table 2S). Loadings of Al and Si on the membrane were lower with PACl-71s pretreatment than with PACl-51s pretreatment (Fig. 3S, Supplementary data). Therefore, the lower TMP rise observed with PACl-71s pretreatment could possibly be due to lower loading rates of compounds composed of these elements.

The residual aluminum in the filtrate was lower with PACl-71s pretreatment than with PACl-51s pretreatment (Runs 2–5 of Fig. 4: the comparison in Run 1 was not appropriate because pH was not stable during the experiment and pH of PACl-71s coagulation was often higher than pH of PACl-51s coagulation). This was due to less monomeric aluminum (Ala) in PACl-71s [17]; the percentages of Ala in PACl-71s and PACl-51s are 18.3% and 43.5%, respectively (Table 1S, Supplementary data). Similar residual aluminum results were also seen in the filtrates of the manually collected samples through a polycarbonate membrane, which did not exhibit adsorption ability, with fixed straight pores of the size 0.1 μm, the same as that of the ceramic membrane [19] (Fig. 4S, Supplementary data). Therefore, it can be interpreted that the concentration of

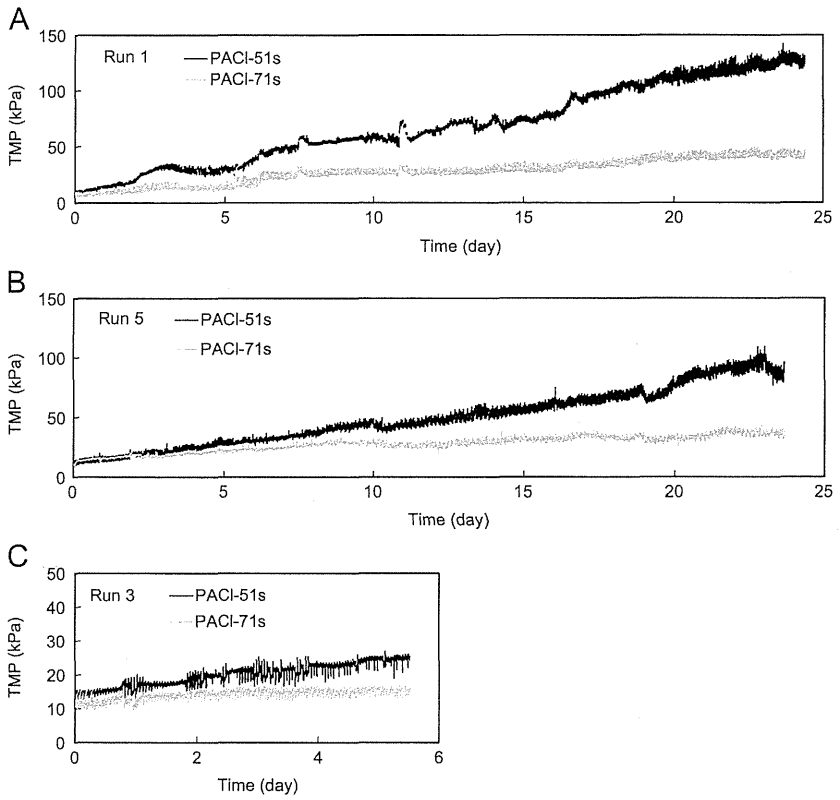

Fig. 2. Comparison of TMP variations during microfiltration after PACl-51s and PACl-71s coagulations: (A) Run 1 (coagulation pH 6.1–7.3); (B) Run 5 (coagulation pH 7.0); (C) Run 3 (coagulation pH 7.5).

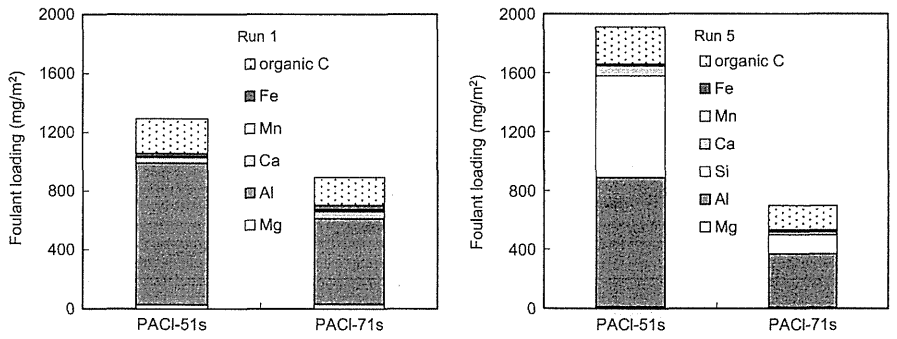

Fig. 3. Elemental compositions of membrane foulants recovered in chemical cleaning agents (Si was not analyzed for Run 1).

small-size aluminum passing through the ceramic membrane was lower with PACl-71s pretreatment than with PACl-51s pretreatment. Some of the small-size aluminum species passing through the membrane pores might be retained by chance in membrane pores and then foul the membrane. We then thought that the low extent of membrane fouling with PACl-71s pretreatment might have been related to a low aluminum concentration. Molecular weight fractionation with organic MF and UF membranes revealed that the difference in aluminum concentration in the filtrates with the PACl-71s and PACl-51s pretreatments was in the size range > 500 Da (Fig. 5S, Supplementary data). This result is in accordance with previous jar test results that showed that PACl-71s lowered residual aluminum in the size range > 500 Da [17]. The DOC in the filtrate was also lower with PACl-71s pretreatment than with PACl-51s pretreatment (Fig. 6S), and the loadings of organic carbon on the membrane were lower with PACl-71s pretreatment than with PACl-51s pretreatment (Fig. 3S). Therefore,

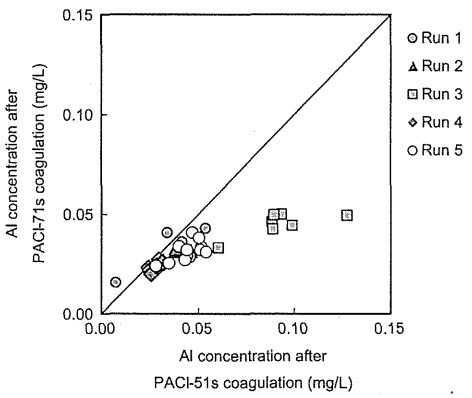

Fig. 4. Aluminum concentrations in the MF filtrates after PACl-71s and PACl-51s coagulations.

the high NOM removal capability of PACl-71s might also be related to the low rate of TMP buildup.

3.2. Effect of very-high-basicity (90%) PACl

We tested two very-high-basicity (90%) PACls (PACl-90b and PACl-90). PACl-90b had a higher content of Alb, which has a high charge neutralization capacity [20,21], than PACl-90 or PACl-71s. Kimura et al. [17] reported that very-high-basicity (90%) PACls can decrease the residual Al concentration much more than 71% basicity PACls because 90%-basicity PACls only contain a very small amount of monomeric aluminum species (Ala). Given the lower TMP rise of PACl-71s with respect to PACl-51s, it was suspected that the extent of membrane fouling was related to residual Al concentration in the filtrate, with lower residual leading to lower fouling and less TMP buildup. The percentages of Ala in PACl-90, PACl-90b, PACl-71s, and PACl-51s are 0.4%, 1.2%, 18.3%, and 43.5%, respectively (Table 1S). Therefore, membrane fouling should be less with PACl-90b and PACl-90 than with PACl-71s. Three pairs of runs were carried out. Results for two pairs of the runs are shown in Fig. 5, and results for the third pair, which had a shorter operational time, are shown in Fig. 7S (Supplementary data). In all runs, coagulations with PACl-90b and PACl-90 yielded a similar TMP buildup over the entire operation time as coagulation with PACl-71s. Nonsulfated PACls of basicities 71% and 90% (PACl-71 and PACl-90) also saw no difference in TMP buildup (Fig. 8S, Supplementary data). Loadings of Al on the membrane were not different between PACls with basicities of 90% (PACl-90 and PACl-90b) and 71% (PACl-71s) (Fig. 9S, Supplementary data).

While further reduction of the residual aluminum concentration (< 0.009 mg/L) was successfully achieved – as expected, aluminum concentrations in the filtrates dramatically decreased as basicity increased from 71% to 90% (Fig. 6) – it was not accompanied by a further attenuation of TMP buildup. Thus, increasing basicity to 90% and changing the aluminum species distribution did not further improve permeability. This result suggests that the quantity of small-size aluminum species passing through the membrane pores was not the main cause of the membrane's fouling. Instead, the aluminum species that did not pass through the membrane pores might have caused external membrane fouling by forming a gel layer, which probably consisted mostly of aluminum, on top of the separation layer of the membrane. This differs from pretreatment with a PACl with a basicity of 51%, where external membrane fouling may have been caused by formation of a gel layer and internal membrane fouling could have been caused by internal deposition of aluminum associated with particles smaller than the membrane pore size. Therefore, the characteristics of the membrane foulant might depend on the basicity of the PACl used for coagulation pretreatment. The DOC in the filtrate was slightly higher with 90%-basicity PACl pretreatment than with 71% pretreatment (Fig. 10S). The loading of organic carbon was also slightly higher with 90%-basicity PACl pretreatment. Therefore, the effect of the low aluminum concentration with 90%-basicity PACls might possibly be canceled out with its high DOC, which eventually resulted in the similar TMP buildup rate of PACl-90 to PACl-71s. Experiments using raw water of high NOM concentration are granted to more clearly elucidate the effect of PACl characteristics on the NOM removal and fouling [22].

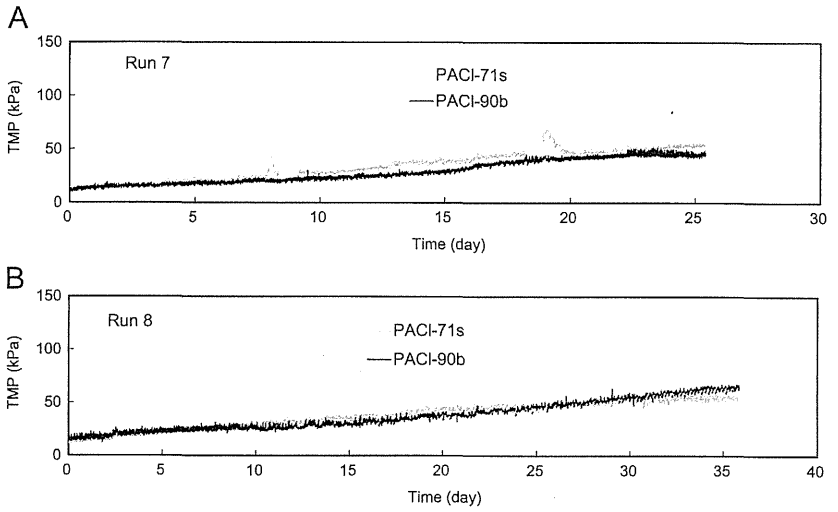

Fig. 5. Comparison of TMP variations during microfiltration after PACl-90b and PACl-71s coagulations: (A) Run 7 (coagulation pH 7.5); (B) Run 8 (coagulation pH 7.5).

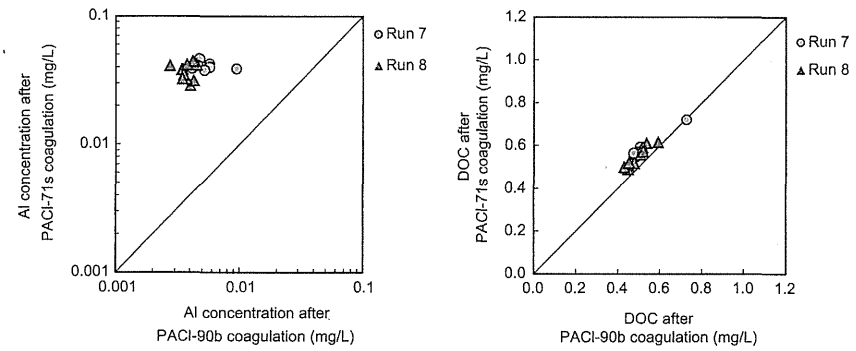

Fig. 6. Aluminum and DOC concentrations in the MF filtrates after PACl-90b and PACl-71s coagulations.

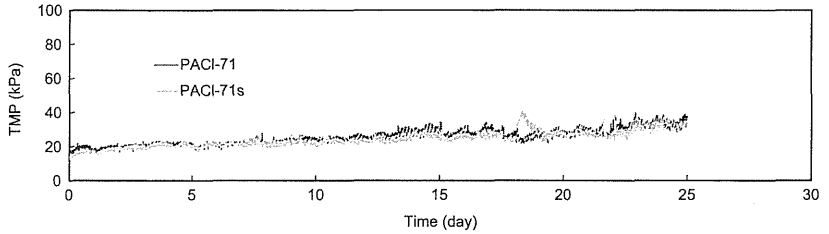

Fig. 7. Comparison of TMP variations during microfiltration after PACl-71 and PACl-71s coagulations. Run 11 (coagulation pH 7.5).

3.3. Effect of sulfate ion in PACl

Sulfate is often added to PACls because it suppresses charge reversal and enhances flocculation performance [25]. Pretreatment with PACl-90b produced very fine floc particles, whereas pretreatment with PACl-71s produced larger floc particles (Fig. 11S, Supplementary data). The very fine floc particles formed by PACl-90b are probably due to the absence of sulfate ion in the PACl. Therefore, it seemed likely that pretreatment with very-high-basicity (90%) PACls would cancel out the positive effect from the lower residual Al concentration with a possible negative effect from the very fine floc particles.

To further study the effect of floc size on filtration, we compared PACl-71s and PACl-71 – two PACls with the same basicity and aluminum species distribution but with or without the sulfate ion in their structures (Table 1S). PACl-71 formed more very fine floc particles than did PACl-71s (Fig. 12S, Supplementary data), however, the TMP variations during filtration were similar (Fig. 7). This result indicates that the very fine floc particles formed by the nonsulfated PACls (PACl-90b and PACl-71) did not have a negative impact on the irreversible fouling, leaving only the positive effect of TMP mitigation. This is further supported by microphotographs that show particles larger than a few microns, much larger than the membrane pore size (0.1 μm), and therefore would not plug the membrane pores. Lastly, the chemical constitution of the irreversible foulant was different from that of the floc particles (see Section 3.4) thus floc particles were not directly related to the irreversible fouling. Here we would like to note that our results of the little floc-size effect were obtained on the experiments of dead-end mode filtration. For other hydro-dynamic conditions, such as cross-flow mode, the further study is needed.

So far, the results can be generalized as follows: for a MF system that includes an intensive hydraulic backwash process, coagulants that produce floc particles much larger than the membrane pore size are more than enough for pretreatment. Such a coagulant property is actually required for pretreatment before sedimentation or for enhancing cake layer permeability in membrane systems without a hydraulic backwash. We therefore infer that a high-basicity nonsulfated PACl functions successfully as such a coagulant provided that it retains the capacity to neutralize charge.

Furthermore, inclusion of sulfate ions in PACls with high aluminum content influences the PACls' long-term chemical stability, so the sulfate ion concentration in practically applied PACls with Al content $>5\%$ (w/w) is typically limited to a few percent to allow the storage periods >6 months. Therefore, the success of the high-basicity nonsulfated PACl gives merit to its practical application in terms of a long storage period.

3.4. Aluminum and silicate loads on membrane

The spent membrane-cleaning solutions from filtration runs, including short runs terminated forcibly by cessation of raw water supply, were analyzed for the major irreversible membrane foulants, Al and Si. The ratios of Si/Al were plotted against the basicity of the PACls used for the coagulation pretreatment (Fig. 8). The Si/Al ratios decreased with increasing basicity, suggesting that the characteristics of the membrane foulant differ depending on the basicity of PACl used for the coagulation pretreatment. Therefore, we infer that increasing the PACl basicity not only decreases the concentration of aluminum passing through the membrane and thereby possibly reducing the load of the major foulant, aluminum, but also it changes the characteristics of membrane foulant and through this, may contribute to the attenuation of the TMP buildup.

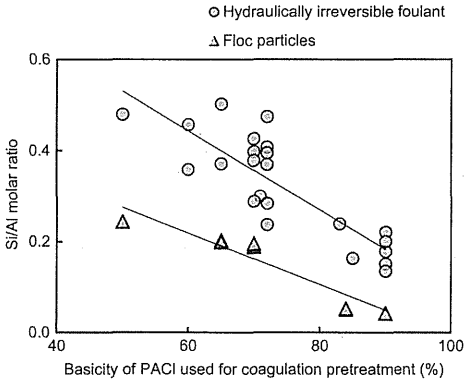

Fig. 8. Comparison of Si/Al molar ratios (Runs 6–9, 11, 12 and 17–19. Coagulation pH was 7.5–7.8).

The feed water to the membrane contained aluminum and silicate at very different concentrations. The aluminum concentration (around 1.2 mg/L on average) was much lower than the Si concentration (around 6.6 mg/L), and the Si/Al molar ratio was about 5.3 for the feed water. The Si/Al ratios of the irreversible membrane foulant varied from 0.5 to 0.2, depending on the basicity of the PACls. Since most of the aluminum in the feed water to the membrane was in a suspended form (floc), whereas the silicate was in a soluble form, a small portion of the silicate might have been incorporated into the aluminum that precipitated after the PACl was dosed. However, the extent of incorporation is low for high-basicity PACl because the aluminum was pre-neutralized in the PACl solution. The Si/Al ratio of the irreversible membrane foulant at each basicity was also higher than that of the floc particles that were ejected by the hydraulic backwash, the highest ratio of which was 0.2. The difference of the Si/Al ratio suggests that the irreversible foulant did not originate from floc particles, even though the irreversible foulant also consisted mostly of aluminum. Adding to the fact that floc size did not affect the extent of irreversible fouling, this further shows that floc particles are not directly related to irreversible fouling.

The higher Si/Al ratios of the irreversible foulant for the lower-basicity PACls suggest that Si plays a role in membrane fouling. A stability diagram (Geochemist's Workbench, ver. 6, RockWare, Inc., Golden, CO, USA) for the chemistry of the membrane feedwater suggests that kaolinite [$Al_2Si_2O_5(OH)_4$] was the final stable species; the aqueous solubility of kaolinite is much lower than that of gibbsite [$Al(OH)_3$] [23]. The Si/Al molar ratio of kaolinite is 1.0, a value closer to

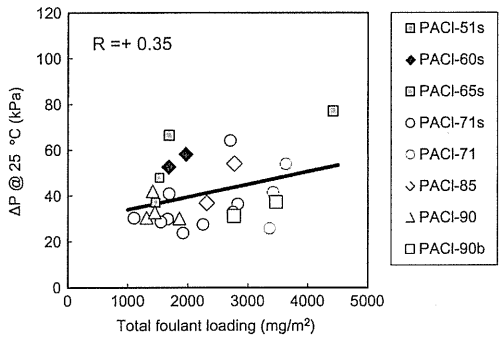

Fig. 9. Relationship between TMP normalized at 25 °C and foulant loading (Runs 5–9, 11, 12 and 17–19). The total foulant loading was calculated with the assumption that Al and Si mainly exist in the forms of $Al_2Si_2O_5(OH)_4$ according to Section 3.1, the excess Al in the form of $Al(OH)_3$ if Al/Si > 1, the excess Si in the form of SiO_2 if Si/Al > 1, Ca in the form of $Ca(OH)_2$, Mg in the form of $Mg(OH)_2$, Fe in the form of $Fe(OH)_3$, and Mn in the form of $MnO(OH)_2$; the carbon content of organic matter was 51%.

that of the irreversible foulant than to that of the floc particles. We infer that aluminum silicate hydroxide, which is chemically similar to kaolinite but amorphous, probably accumulated on top of and inside the membrane, thereby irreversibly fouling the membrane.

Quantification of total foulant loads sheds light on its relationship to TMP rise; however, it requires information about the chemical structures of the foulants and such information is scant. The total loads shown in Fig. 9 were calculated on the assumption that the Si existed mainly in compounds characterized by the stoichiometry of $Al_2Si_2O_5(OH)_4$, the surplus of Al over Si was in the form of $Al(OH)_3$, Ca was in the form of $Ca(OH)_2$, Mg was in the form of $Mg(OH)_2$, Fe was in the form of $Fe(OH)_3$, and Mn was in the form of $MnO(OH)_2$. Carbon was assumed to account for 50% of the organic matter [24]. The positive correlation between the total foulant loading and TMP suggests that the quantity of total foulant loading is an index for TMP. However, the correlation was not high ($r = +0.35$, Fig. 9). When compared at the same loading, the TMPs of direct MF after coagulation with normal basicities (50% and 60%) were higher than the TMPs associated with high and very-high basicities (> 70%). This correlation suggests the rise in TMP may to some extent be related to the quantity of total foulant loading on the membrane, but altogether, the characteristics of membrane foulants depend primarily on the PACls used for coagulation pretreatment.

4. Summary

1) In ceramic MF with PACl coagulation pretreatment, long-term development of TMP caused by hydraulically irreversible fouling followed the order PACl-90b=PACl-90=PACl-71s < PACl-51s. Use of high-basicity (71%) PACl coagulant (PACl-71s) reduced hydraulically irreversible fouling and attenuated long-term development of TMP compared with normal-basicity (51%) PACl coagulants (PACl-51s). The use of very-high-basicity (90%) PACls (PACl-90b and PACl-90), however, did not result in a reduction of long-term TMP buildup beyond that obtained with PACl-71s.
2) Aluminum concentrations in the filtrates were in the following order: PACl-90=PACl-90b < PACl-71s < PACl-51s. This order paralleled the order of Ala content in the PACls. The lower aluminum passage following pretreatment with a high-basicity PACl correlated with less membrane fouling. PACl-90 and PACl-71s exhibited similar long-term TMP buildup, suggesting that the characteristics of the membrane foulant differed from the normal basicity PACl of 51%. This conclusion was also supported by the fact that the Si/Al ratio of hydraulically irreversible foulants, which consisted mostly of Al and Si, decreased with increasing basicity of the PACl used for coagulation pretreatment.
3) The hydraulically irreversible foulants differed in terms of Si/Al ratios compared to floc particles. Additionally, while floc size was a function of the concentration of sulfate ions and polymeric species in the PACls, it did not affect the reduction of hydraulically irreversible fouling. Therefore, the floc particles were not directly related to hydraulically irreversible fouling.

Acknowledgments

This study was supported by a Grant-in-Aid for Scientific Research S (24226012) from the Japan Society for the Promotion of Science.

Appendix A. Supporting information

Supplementary data associated with this article can be found in the online version at http://dx.doi.org/10.1016/j.memsci.2014.12.033.

References

[1] H. Huang, K. Schwab, J.G. Jacangelo, Pretreatment for low pressure membranes in water treatment: a review, Environ. Sci. Technol. 43 (2009) 3011–3019.
[2] Y. Matsui, T. Matsushita, T. Inoue, M. Yamamoto, Y. Hayashi, H. Yonekawa, Y. Tsutsumi, Virus removal by ceramic membrane microfiltration with coagulation pretreatment, Water Sci. Technol. 3 (2003) 93–99.
[3] W. Xu, B. Gao, Effect of shear conditions on floc properties and membrane fouling in coagulation/ultrafiltration hybrid process—the significance of Alb species, J. Membr. Sci. 415–416 (2012) 153–160.
[4] W. Xu, B. Gao, Y. Wang, Q. Zhang, Q. Yue, Influences of polysilicic acid in Alb species on floc properties and membrane fouling in coagulation/ultrafiltration hybrid process, Chem. Eng. J. 181–182 (2012) 407–415.
[5] Y. Matsui, H. Hasegawa, K. Ohno, T. Matsushita, S. Mima, Y. Kawase, T. Aizawa, Effects of super-powdered activated carbon pretreatment on coagulation and trans-membrane pressure buildup during microfiltration, Water Res. 43 (2009) 5160–5170.
[6] M.H. Cho, C.H. Lee, S. Lee, Influence of floc structure on membrane permeability in the coagulation–MF process, Water Sci. Technol. 51 (2005) 143–150.
[7] Y.H. Choi, H.S. Kim, J.H. Kweon, Role of hydrophobic natural organic matter flocs on the fouling in coagulation–membrane processes, Sep. Purif. Technol. 62 (2008) 529–534.
[8] B. Zhao, D. Wang, T. Li, C. Huang, Effect of floc structure and strength on membrane permeability in the hybrid coagulation-microfiltration process, Water Sci. Technol. 11 (2011) 97–105.
[9] J. Wang, J. Guan, S.R. Santiwong, T.D. Waite, Characterization of floc size and structure under different monomer and polymer coagulants on microfiltration membrane fouling, J. Membr. Sci. 321 (2008) 132–138.
[10] T. Liu, Z.-l. Chen, W.-Z. Yu, J.-m. Shen, J. Gregory, Effect of two-stage coagulant addition on coagulation–ultrafiltration process for treatment of humic-rich water, Water Res. 45 (2011) 4260–4268.
[11] T.D. Waite, A.I. Schäfer, A.G. Fane, A. Heuer, Colloidal fouling of ultrafiltration membranes: impact of aggregate structure and size, J. Colloid Interface Sci. 212 (1999) 264–274.
[12] E. Barbot, S. Moustier, J. Bottero, P. Moulin, Coagulation and ultrafiltration: understanding of the key parameters of the hybrid process, J. Membr. Sci. 325 (2008) 520–527.
[13] B. Zhao, D. Wang, T. Li, C.W.K. Chow, C. Huang, Influence of floc structure on coagulation–microfiltration performance: effect of Al speciation characteristics of PACls, Sep. Purif. Technol. 72 (2010) 22–27.
[14] W. Yu, T. Liu, J. Gregory, L. Campos, G. Li, J. Qu, Influence of flocs breakage process on submerged ultrafiltration membrane fouling, J. Membr. Sci. 385–386 (2011) 194–199.
[15] Y. Chen, B.Z. Dong, N.Y. Gao, J.C. Fan, Effect of coagulation pretreatment on fouling of an ultrafiltration membrane, Desalination 204 (2007) 181–188.
[16] T. Tran, S. Gray, R. Naughton, B. Bolto, Polysilicato-iron for improved NOM removal and membrane performance, J. Membr. Sci. 280 (2006) 560–571.
[17] M. Kimura, Y. Matsui, K. Kondo, T.B. Ishikawa, T. Matsushita, N. Shirasaki, Minimizing residual aluminum concentration in treated water by tailoring properties of polyaluminum coagulants, Water Res. 47 (2013) 2075–2084.
[18] D. Wang, W. Sun, Y. Xu, H. Tang, J. Gregory, Speciation stability of inorganic polymer flocculant–PACl, Colloids Surf. A 243 (2004) 1–10.
[19] Y. Matsui, T.B. Ishikawa, M. Kimura, K. Machida, N. Shirasaki, T. Matsushita, Aluminum concentrations of sand filter and polymeric membrane filtrates: a comparative study, Sep. Purif. Technol. 119 (2013) 58–65.

[20] B.-Y. Gao, Y.-B. Chu, Q.-Y. Yue, B.-J. Wang, S.-G. Wang, Characterization and coagulation of a polyaluminum chloride (PAC) coagulant with high Al13 content, J. Environ. Manag. 76 (2005) 143–147.
[21] N. Parthasarathy, J. Buffle, Study of polymeric aluminium(III) hydroxide solutions for application in waste water treatment. Properties of the polymer and optimal conditions of preparation, Water Res. 19 (1985) 25–36.
[22] H. Zhao, H. Liu, C. Hu, J. Qu, Effect of aluminum speciation and structure characterization on preferential removal of disinfection byproduct precursors by aluminum hydroxide coagulation, Environ. Sci. Technol. 43 (2009) 5067–5072.
[23] K. Ohno, Y. Matsui, M. Itoh, Y. Oguchi, T. Kondo, Y. Konno, T. Matsushita, Y. Magara, NF membrane fouling by aluminum and iron coagulant residuals after coagulation–MF pretreatment, Desalination 254 (2010) 17–22.
[24] International Humic Substance Society, Elemental Compositions and Stable Isotopic Ratios of IHSS Samples, 2013.
[25] A. Amirtharaja, C.R. O'Melia, Coagulation processes: destabilization, mixing, and flocculation, in: F.W. Pontius (Ed.), Water Quality & Treatment, 4th ed., McGraw-Hill, 1990.

WATER RESEARCH 68 (2015) 227–237

Available online at www.sciencedirect.com

ScienceDirect

journal homepage: www.elsevier.com/locate/watres

Removal of iodide from water by chlorination and subsequent adsorption on powdered activated carbon

Mariya Ikari [a], *Yoshihiko Matsui* [b,*], *Yuta Suzuki* [a], *Taku Matsushita* [b], *Nobutaka Shirasaki* [b]

[a] *Graduate School of Engineering, Hokkaido University, N13W8, Sapporo 060-8628, Japan*
[b] *Faculty of Engineering, Hokkaido University, N13W8, Sapporo 060-8628, Japan*

ARTICLE INFO

Article history:
Received 5 June 2014
Received in revised form
7 October 2014
Accepted 8 October 2014
Available online 16 October 2014

Keywords:
Iodide
Iodate
SPAC
PAC
NOM

ABSTRACT

Chlorine oxidation followed by treatment with activated carbon was studied as a possible method for removing radioactive iodine from water. Chlorination time, chlorine dose, the presence of natural organic matter (NOM), the presence of bromide ion (Br^-), and carbon particle size strongly affected iodine removal. Treatment with superfine powdered activated carbon (SPAC) after 10-min oxidation with chlorine (1 mg-Cl_2/L) removed 90% of the iodine in NOM-containing water (dissolved organic carbon concentration, 1.5 mg-C/L). Iodine removal in NOM-containing water increased with increasing chlorine dose up to 0.1 mg-Cl_2/L but decreased at chlorine doses of >1.0 mg-Cl_2/L. At a low chlorine dose, nonadsorbable iodide ion (I^-) was oxidized to adsorbable hypoiodous acid (HOI). When the chlorine dose was increased, some of the HOI reacted with NOM to form adsorbable organic iodine (organic-I). Increasing the chlorine dose further did not enhance iodine removal, owing to the formation of nonadsorbable iodate ion (IO_3^-). Co-existing Br^- depressed iodine removal, particularly in NOM-free water, because hypobromous acid (HOBr) formed and catalyzed the oxidation of HOI to IO_3^-. However, the effect of Br^- was small in the NOM-containing water because organic-I formed instead of IO_3^-. SPAC (median particle diameter, 0.62 μm) had a higher equilibrium adsorption capacity for organic-I than did conventional PAC (median diameter, 18.9 μm), but the capacities of PAC and SPAC for HOI were similar. The reason for the higher equilibrium adsorption capacity for organic-I was that organic-I was adsorbed principally on the exterior of the PAC particles and not inside the PAC particles, as indicated by direct visualization of the solid-phase iodine concentration profiles in PAC particles by field emission electron probe microanalysis. In contrast, HOI was adsorbed evenly throughout the entire PAC particle.

* *Corresponding author.* Tel./fax: +81 11 706 7280.
E-mail address: matsui@eng.hokudai.ac.jp (Y. Matsui).
http://dx.doi.org/10.1016/j.watres.2014.10.021
0043-1354/